Accepted Manuscript

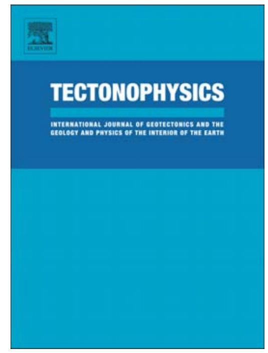

Gaps, tears and seismic anisotropy around the subducting slabs of the Antilles

David Schlaphorst, J-Michael Kendall, Brian Baptie, Joan L. Latchman, Steve Tait

PII: S0040-1951(17)30002-1
DOI: doi:10.1016/j.tecto.2017.01.002
Reference: TECTO 127374

To appear in: *Tectonophysics*

Received date: 3 August 2016
Revised date: 11 December 2016
Accepted date: 3 January 2017

Please cite this article as: Schlaphorst, David, Kendall, J-Michael, Baptie, Brian, Latchman, Joan L., Tait, Steve, Gaps, tears and seismic anisotropy around the subducting slabs of the Antilles, *Tectonophysics* (2017), doi:10.1016/j.tecto.2017.01.002

Gaps, Tears and Seismic Anisotropy around the Subducting Slabs of the Antilles

David Schlaphorst*[1], J-Michael Kendall[1], Brian Baptie[2], Joan L. Latchman[3], Steve Tait[4]

(*corresponding author)

[1]School of Earth Sciences, University of Bristol, Bristol, UK.

[2]British Geological Survey, Edinburgh, UK.

[3]Seismic Research Centre, The University of the West Indies, St. Augustine, Trinidad & Tobago.

[4]Institut de Physique du Globe de Paris, Paris, France.

Emails:

David Schlaphorst: david.schlaphorst@bristol.ac.uk

J-Michael Kendall: gljmk@bristol.ac.uk

Brian Baptie: bbap@bgs.ac.uk

Joan L. Latchman: j_latchman@uwiseismic.com

Steve Tait: tait@ipgp.fr

Abstract

Seismic anisotropy in and beneath the subducting slabs of the Antilles is investigated using observations of shear-wave splitting. We use a combination of teleseismic and local events recorded at three-component broadband seismic stations on every major island in the area to map anisotropy in the crust, the mantle wedge and the slab/sub-slab mantle. To date this is the most comprehensive study of anisotropy in this region, involving 52 stations from 8 seismic networks. Local event delay times (0.21±0.12s) do not increase with depth, indicating a crustal origin in anisotropy and an isotropic mantle wedge. Teleseismic delay times are much larger (1.34±0.47s), with fast shear-wave polarisations that are predominantly parallel to trend of the arc. These observations can be interpreted three ways: (1) the presence of pre-existing anisotropy in the subducting slab; (2) anisotropy due to sub-slab mantle flow around the eastern margin of the nearly stationary Caribbean plate; (3) some combination of both mechanisms. However, there are two notable variations in the trench-parallel pattern of anisotropy - trench-perpendicular alignment is observed in narrow regions east of Puerto Rico and south of Martinique. These observations support previously proposed ideas of eastward sublithospheric mantle flow through gaps in the slab. Furthermore, the pattern of anisotropy south of Martinique, near Saint Lucia is consistent with a previously proposed location for the boundary between the North and South American plates.

Keywords: anisotropy, subduction zone, Lesser Antilles

1. Introduction

The degree of coupling between slabs and the convecting mantle is still not fully understood, partly because it is difficult to constrain this from geophysical observations. Flow-induced seismic anisotropy provides arguably one of our best tools to study this and numerous studies suggest that subduction zones cause large-scale redirection of mantle flow around the subducting slab. This is further complicated by slab gaps or tears that lead to slab segmentation, providing potential locations for mantle flow across these tectonic boundaries (Russo & Silver, 1994; Russo et al., 2010). Slab segmentation has been inferred in many subduction environments, such as the Philippine plate beneath central Japan (Mazzotti et al., 1999) and the Ryukyu arc (Lin et al., 2004), central Italy (Rosenbaum et al., 2008), southern Chile (Russo et al., 2010), and the Lesser Antilles Arc (Wadge & Shepherd, 1984; Benthem et al., 2013). Based on the ideas of ten Brink (2005), the effect of a slab tear on seismic anisotropy has also been investigated east of the island of Puerto Rico (Meighan & Pulliam, 2013; Meighan et al., 2013). The 'continental undertow' model (Alvarez, 1982) and its subsequent modification (Alvarez, 2001) propose eastward sublithosphere mantle flow beneath the Caribbean in order to accommodate mantle material redistribution from the shrinking Pacific. However, the outflow would be blocked by the subducting slab beneath the Lesser Antilles. Here we investigate seismic anisotropy along the Lesser Antilles Arc and the tectonic boundary of the adjacent Greater Antilles, assessing the continuity of mantle flow along this complex plate boundary.

Seismic anisotropy leads to variations in the speed of seismic waves as a function of the direction of wave propagation, observations of which can be used to investigate the heterogeneity of anisotropy in the crust and upper-mantle in subduction regions (Russo et al., 1996; Long & van der Hilst, 2006; Di Leo et al., 2012). Seismic anisotropy can be caused by different mechanisms, intrinsic or extrinsic. Intrinsic ones include crystal alignment of anisotropic minerals due to shear strain, called lattice-preferred orientation (LPO; Mainprice & Nicolas, 1989). Large-scale alignment of these minerals, primarily olivine in the upper mantle, will lead to the formation of an anisotropic region. Anisotropy can be also introduced by extrinsic effects, such as thin layering of materials with contrasting elastic properties (Backus, 1962), as well as the alignment of cracks, fractures or inclusions. The alignment of fluid-filled cracks is thought to be a widespread source of anisotropy in the upper crust (Crampin et al., 1980a; 1980b; Silver, 1996, Keir et al., 2005). In such cases, anisotropy occurs due to the alignment of larger-scale features, an effect commonly termed shape-preferred orientation (SPO; Mainprice & Nicolas, 1989). In order to resolve these features, their size has to be smaller than the seismic wavelength used for the observation. Hence, extrinsic effects are dependent on the seismic frequency (Savage, 1999; Al-Harrasi et al., 2011). In the crust an orientation in the direction of maximum stress is observed, commonly being parallel to the alignment of fractures or cracks.

The independent propagation of two shear-waves is a distinct feature of seismic anisotropy and observations of this so-called shear-wave splitting are now used routinely to probe seismic anisotropy in the deep Earth. The length scale of lateral variations in shear-wave splitting can be used to constrain depths of the anisotropic layer by appealing to arguments based on the size of Fresnel Zones of teleseismic phases (Alsina & Snieder, 1995; Hammond et al., 2010). Constraining layers of anisotropy requires a detailed study of shear-wave splitting as a function of the initial source polarisation (Savage & Silver, 1993), which can be posed as a tomographic inverse problem (Wookey, 2012). This problem becomes much easier if there is a good depth distribution of seismic events beneath a region of interest. Fortunately, this is possible in subduction regions, as there is generally abundant seismicity in the overlying crust and in the subducting slab. Splitting observed in these events and distant teleseismic phases can be used to constrain anisotropy in the crust, upper-mantle wedge, subducting slab, and underlying mantle (e.g., Di Leo, et al., 2012).

In many subduction zones a strong trench-parallel orientation of the fast shear-wave axis has been observed using teleseismic events (see Long & Silver (2009) and references therein). However, traditional models using a two-dimensional corner flow, combined with an entrained sub-slab mantle flow predict trench-perpendicular fast splitting directions (Ribe, 1989; Russo & Silver, 1994; Hall et al., 2000; Lowman et al., 2007). Therefore, different models have been proposed to explain the widely observed trench-parallel orientation along subduction zones.

In the mantle wedge, the occurrence of B-type LPO can change the fast orientation to perpendicular to the direction of maximal strain. This can be caused by the presence of water (Jung & Karato, 2001) or high pressure at depths of around 80 to 90 km (Jung et al., 2009). B-type olivine can most likely be found in the forearc mantle and a layer above the subducting slab (Kneller et al., 2005). Katayama et al. (2009) show that it is possible to achieve strong trench-parallel orientations by an alignment of serpentine, as the delay times would be large enough to explain results generally observed in subduction environments. More recently Nagaya et al. (2016) have shown that trench parallel anisotropy in the Ryuku subduction zone can be explained by widespread antigorite in the upper-mantle wedge caused by convection in a hydrated forearc mantle.

In the subducting slab another model appeals to serpentinised cracks that are aligned due to slab bending, which creates a combination of SPO and LPO effects (Faccenda et al., 2008; Healy et al., 2009).

Beneath the subducted lithosphere trench-parallel fast directions can also be produced by the entrainment of an asthenosphere layer with weak azimuthal and strong radial anisotropy (Song & Kawakatsu, 2012). A further model to explain trench-parallel behaviour invokes three-dimensional flow (Lowman et al., 2007) including mantle flow around the edges of the subducting slab due to trench migration (Long & Silver, 2008; 2009).

In this study we investigate seismic anisotropy in the eastern Greater and the Lesser Antilles along an extensive subduction environment, including the crust and the upper mantle as regions of interest. We use data from seismic stations operated by a wide range of agencies, yielding the most comprehensive dataset used to study this region to date. A combination of teleseismic and local events is used to observe and distinguish between anisotropy in the crust, the mantle wedge and the sub-slab mantle. We test the Alverez (1982; 2001) model of mantle flow through tears or gaps in the slabs of the eastern Caribbean. The subduction of a plate boundary could lead to a gap in the slab (van Benthem et al., 2013), thus allowing for mantle flow to pass through the gap. Therefore, we can also look for evidence of the boundary between the North American and South American plates, which must be located somewhere along the Lesser Antilles arc.

2. Tectonic Setting

Our study area includes the eastern Greater Antilles and the Lesser Antilles (Figure 1). The eastern Greater Antilles area consists of the Northern Caribbean Plate Boundary Zone (NCPBZ) and includes Hispaniola and Puerto Rico. The tectonic setting of this region is dominated by a left-lateral east-west strike-slip motion. It includes an oblique convergence of the Bahamas Carbonate Banks, a part of the Bahamas ridge, and a pull-apart basin in the Mona Passage, the sea gate between Hispaniola and Puerto Rico (Masson & Scanlon, 1991; Dolan et al., 1998; ten Brink, 2005). The islands themselves are located on microplates, which form a bridge between two subduction zones in close proximity. The oceanic lithosphere of the North American plate subducts at the Puerto Rico trench north of the islands and the thickened Caribbean plate subducts at the Los Muertos trench to the south of Puerto Rico and the eastern part of Hispaniola Dolan et al. (1998). The northern part of Hispaniola undergoes a collision with the southeastern extension of the Bahamas ridge system at the Bahamas Carbonate Banks, which has been ongoing for the last 4 to 5 Ma. This collision caused an opening of the Mona Passage. Due to the highly oblique collision of the northwestern corner of Puerto Rico with the southeastern end of the Bahamas ridge, a counterclockwise motion of the Puerto Rico microplate of around 25° was initiated during the late Miocene (11–4.5 Ma; Reid et al., 1991). Furthermore, a study of the thickness of the carbonate layers off the coast of

Puerto Rico (ten Brink, 2005) revealed that the island experienced an uplift of about 1300 m in the last 3 Ma.

The Lesser Antilles arc is the eastern boundary of the Caribbean plate. It is characterised by a chain of volcanic islands extending from Anguilla and Saba in the north, to the South American continent with Grenada being the southernmost volcanic island. The arc originated from the relatively slow subduction (~ 2 cm/yr; DeMets et al., 2000) of the North and South American plates beneath the Caribbean plate. The subduction of the oceanic South American lithosphere continues to the south where the slab is detached and overridden by the South American continent, leaving a mantle between the continent and the slab that is mobile enough (e.g., not cratonic) to enable the detached slab to retain its position beneath the continent (VanDecar et al., 2003). North of Martinique it bifurcates with an active inner arm including the islands of Montserrat, St. Kitts, St. Eustatius and Saba to the west and an inactive outer arm including the islands of Antigua and St. Martin to the east. Bouysse (1988) and Bouysse et al. (1990) suggest that the underplating of a subducting buoyant ridge blocked the subduction, which led to a jump of the volcanic front to the east at the end of the Palaeogene.

In the west the arc is bounded by the sedimentary Grenada Basin, formed by back-arc spreading, and the Aves Ridge, a remnant arc located 200 km off the LAA (Tomblin, 1975; Stein et al., 1982). In its southern part the Tobago Basin neighbours the arc to the east (Christeson et al., 2008).

In general, earthquakes in the Greater and Lesser Antilles do not occur at great depths; the seismicity can be traced down along the slab to depths of about 200 km, with the average seismicity being at depths of around 100 km beneath the island arc (Westbrook, 1975; Wadge & Shepherd 1984; Westbrook et al., 1984; Schlaphorst et al., 2016). South of Saint Lucia (~13°N) a region of reduced seismicity can be observed (Wadge & Shepherd, 1984). The location of the North America–South America–Caribbean triple junction remains unclear and cannot be observed using focal mechanisms of shallow events (Stein et al., 1982).

Location estimates range from 13°N to 19°N based on gaps in the Wadati-Benioff zone (Wadge & Shepherd, 1984), isostatically uncompensated ridges (Müller & Smith, 1993), seismicity (Bird, 2003) or P-wave velocity tomography models (Benthem et al, 2013).

3. Method

Anisotropy in the subsurface can be investigated through observations of shear-wave splitting. An initially linearly polarised shear-wave splits into two orthogonally polarised shear-waves that have different speeds as they propagate through an anisotropic medium. In this work shear-wave splitting is measured using the approach introduced by Silver & Chan (1991) and extended by Teanby et al. (2004). The style of anisotropy can be described by the polarisation of the fastest shear-wave (φ) and the difference in arrival times between the fast and the slow shear-wave (δt) – the so-called splitting parameters. If δt is smaller than the dominant seismic wavelength the S-wave particle motion will exhibit a characteristic elliptical particle motion, the ellipticity of which can be described by a co-variance matrix. The splitting analysis involves a correction that removes the effects of splitting, which minimises the second eigenvalue of the covariance matrix. If successful, the correction linearises the S-wave splitting particle motion revealing the polarisation of the initial isotropic shear-wave.

Confidence in the splitting parameters linearising the particle motion can be estimated using a statistical F test, which is plotted as an error surface over the grid of δt and φ. Teanby et al. (2004) showed that the splitting result can be highly dependent on the choice of the start and end of this time window, and so modified the method by introducing a range of start and end times, rather than fixed values. Using cluster analysis the method finds solutions that are stable over a large range of different time windows. The solution with the smallest uncertainties within the largest cluster is used as the best solution.

A high SNR on both the radial and transverse component is needed to detect shear-wave splitting (e.g., Restivo & Helffrich, 1999). Bandpass filtering can be useful to increase the SNR. However, the frequency content of teleseismic events lies in a similar range to that of oceanic noise (Webb, 1991). This reduces the improvement of data through filtering, especially at island stations. Furthermore, an increase in attenuation, observed in subduction environments and attributed to the dewatering of the subducted slab (Haberland & Rietbrock, 2001), can also lower the quality of the S-wave phases. Therefore, we stack the contour plots of shear-wave splitting error-surfaces for teleseismic events detected at one or more stations in close proximity, which improves confidence in the results (Wolfe & Silver, 1998). The robustness of the stacked result is increased by introducing a weighting factor that correlates with the SNR (Restivo & Helffrich, 1999).

A single shear-wave splitting observation is most easily interpreted in terms of a single homogeneous anisotropic layer with hexagonal symmetry and a horizontal symmetry axis. Especially for teleseismic events that travel the entire mantle beneath the receiver this assumption may not be true, as complications can arise due to a dipping symmetry axis, lateral and vertical variations in the anisotropy or a lower form of symmetry (e.g., orthorhombic). These effects are revealed through a dependency on initial source polarisation in the splitting parameters (Silver & Savage, 1994; Kendall, 2000). To distinguish between different layers of anisotropy local events can be used, as they do not travel the entire crust and mantle. By including these it is possible to gain insight into the depth dependency on shear-wave splitting results and, thus, to potentially estimate depths of different anisotropic layers. With a combined use of local and teleseismic events it is possible to observe anisotropy in the crust, the upper mantle wedge, the slab and the sub-slab mantle (e.g., Di Leo et al., 2012).

An SKS-wave travels as a P-wave through the outer core, losing the initial source polarisation of the wave. Upon re-entering the mantle, the P-to-S-conversion at the CMB polarises the shear-wave in the sagittal plane (i.e., an SV wave). Therefore, for SK(K)S (and PKS) the source polarisation of the shear-wave splitting result should be close to the backazimuth (baz or baz+180˚). If this is not the case, the wave may have encountered complex anisotropy in the deeper mantle (Hall et al., 2004).

The source polarisation of the local S-waves can be diverse and depends on the focal mechanism of the earthquake. For measurements with these phases the depth of the source and its distance to the receiver is of great importance. P-to-S surface reflections can cause waveform effects that can be mistaken for shear-wave splitting effects (Evans, 1984). To avoid distortion of the signal a so-called shear-wave window has to be introduced. This defines a cone shaped area beneath the receiver in which the threshold for the critical inclination angle is smaller than the critical angle to avoid S-to-P-reflections at the surface that can distort the signal. It depends on the Poisson's ratio, but for our purpose it is approximately 35° from the vertical (Evans, 1984; Savage, 1999).

In summary, there are several indicators that can be used as a guide to identify a good shear-wave splitting measurement:

(a) A clear onset of the shear phase is visible in the data (Figure 2A).
(b) The SNR is high (Figure 2A, B).
(c) The second eigenvalue of the covariance matrix that describes the particle motion is noticeably reduced. This can be seen as an amplitude reduction on the corrected transverse component (Figure 2B).
(d) The fast and slow shear-waves are very similar in shape (Figure 2C, top row).
(e) The corrected particle motion in the defined time window should be linearised, whereas the original motion has an elliptic shape (Figure 2C, bottom row).
(f) The contour plot of the grid-search over the splitting parameters showing the amplitude of the second eigenvalue should have a clear minimum with small well-constrained 95% confidence region (Figure 2D, big panel). A periodic behaviour can often be attributed cycle skipping due to bandlimited or noisy data. In those cases several good solutions are visible.
(g) For the measurements using teleseismic XKS phases the source polarisation is close to the backazimuth (Figure 2D, big panel).

(h) The results are constant over changing time windows, both in φ and δt creating a plateau (Figure 2D, upper small panel).
(i) The cluster analysis shows few results outside a distinctive cluster around the best solution in δt–φ space (Figure 2D, lower small panel).

In this study, we use local S-waves originating in the slab and teleseismic SK(K)S-waves, selecting only the events with clear onsets of these phases. The quality of the individual splitting measurements was inspected manually using the indicators listed above. Good splitting measurements fulfil all the listed requirements. As low SNR was the main concern in this study, SNR weighted stacking was used (Wolfe & Silver, 1998). However, it is not possible to stack the local S-wave results due to their varying initial source polarisation. Instead we consider rose diagrams of splitting parameters for regional subcells across the study area. In these diagrams all results within different latitude-longitude ranges are averaged both in time lag and fast polarisation angle, creating a circular histogram.

4. Previous Studies of Seismic Anisotropy in the eastern Caribbean

Previous studies of anisotropy in the eastern Caribbean have used local, teleseismic or source-side shear-wave splitting. These studies show a predominant trench-parallel alignment of the fast shear-wave and mostly agree with each other at common stations.

Russo et al. (1996) investigate teleseismic SKS-, SKKS- and PKS- waves at station SJG on Puerto Rico, as well as stations in Trinidad and Venezuela. An attempt to measure source-side splitting is made, using events from the LAA, but the results are too noisy to be useful. They do not find any influence of the counter-clock rotation of Puerto Rico on their results and attribute the trench-parallel orientation to a sinistral motion at the NA-Ca plate boundary, potentially including a minor transtensional component.

Piñero-Feliciangeli & Kendall (2008) measure shear-wave splitting around the Caribbean plate using teleseismic SKS and SKKS and local S-waves. The seven stations observed in the Greater and Lesser Antilles, SJG (Puerto Rico), FDF (Martinique) and five stations on Montserrat, show a trench-perpendicular orientation of the fast shear-wave. The slab S-wave results show a similar orientation but with much smaller delay times, suggesting that the cause of anisotropy is either in the slab or more likely due to mantle flow beneath the slab.

Benford et al. (2012) use SKS-, SKKS-, PKS- and sSKS-waves from eight stations in the Greater Antilles, STVI on the Virgin Islands and ANWB on Barbuda. Their splitting measurements show fast shear-wave orientations parallel to the boundaries of the microplates, whereas stations located away from the micro plate boundaries, SDD (Hispaniola), SJG and STVI, show either weak splitting or a lack of a single predominant direction. They conclude that the deformation of the upper mantle is confined to the microplate boundaries due to their observation of weaker or missing splitting patterns at stations located tens of kilometres away from those boundaries.

Meighan & Pulliam (2013) investigate the splitting parameters at 28 stations along the Greater Antilles and the LAA. However, stations from the French observatories on Guadeloupe and Martinique, as well as the SRC station on St. Lucia are not included. They work with teleseismic SKS- and SKKS-waves, using individual band-pass filters for each event. In general, the results show trench-parallel alignment of the fast shear-waves for the stations. In the Virgin Islands two stations (ABVI, CDVI) show trench-perpendicular orientations, which they attribute to mantle flow through a slab tear that was observed previously in that region (ten Brink, 2005).

Lynner & Long (2013) use source-side splitting measurements of seismic events in the LAA. Along the LAA they observe a trench-parallel alignment of the fast shear-wave, which they explain with a northward mantle flow beneath the slab. In the southern part of the arc they observe trench-perpendicular orientation that aligns well with the direction of subduction. They argue that the mantle flow is being hindered to migrate around the southern end of the slab by a thick South American lithospheric root. Therefore, the deviation of trench-parallel orientation in the south is likely to be caused by local trench-perpendicular stretching due to trench migration or local entrained sub-slab flow from an efficient coupling of the slab and the mantle. This finding is consistent with the pattern observed by Russo et al. (1996) around the northern coast of South America.

Hodges & Miller (2013) were able to confirm the trench-parallel orientation in the Greater Antilles and northern Lesser Antilles by investigating splitting parameters at 19 stations. However, in contrast to Meighan & Pulliam (2013) they did not find trench-perpendicular orientations at stations ABVI and CDVI. They conclude that there is no slab tear to be found in the vicinity of these islands or that the tear is either too narrow or too short-lived.

5. Data

To assess differences in the anisotropic nature of the region, 52 stations from local seismic networks were used in this study to carry out shear-wave splitting measurements. To date this is the most comprehensive study of anisotropy in this region. Of these stations 16 are run by the Puerto Rico Seismic Network, 12 were previously operated by the British Geological Survey, 9 by the West Indies French Seismic Network, 5 by the Eastern Caribbean Seismograph Network, 4 by the USGS Global Seismic Network, 3 by the Netherlands Antilles Seismic Network, 2 by the Dominican Republic Seismic Network and 1 by GEOSCOPE. All of these stations are three-component broadband stations, located on the major islands along the NCPBZ and the LAA.

The teleseismic events were chosen to have an epicentral distance of 85° to 135° (Figure 3A), where the SKS-wave is isolated from other phases (Silver, 1996), and a magnitude larger than 5.6. At greater distances SKS will start to interfere with the inner core boundary, whereas at shorter distances it interferes with S and ScS arrivals.

The local events were taken from seismic catalogues provided by the USGS, the SRC and the IPGP (see Figure 3B for a depth histogram). The epicentres of local events are located close to the station, so that the incidence angle falls within the shear-wave window.

The SNR was improved using butterworth bandpass filters between 0.03 Hz and 0.4 Hz for the teleseismic events. For the station from the French networks it was not possible to observe good splitting measurements with these filter boundaries. Therefore, corner frequencies of 0.01 Hz and 0.1 Hz were chosen.

In general, data quality is highly variable. For the local events, spectra of noise and signal revealed a reduced frequency content around 3 Hz for some stations. At higher frequencies the shear-wave splitting method tends to become unstable due to the insufficient sampling rate of many data. Therefore, the corners were chosen to be at and 0.5 Hz and 2.5 Hz. To further check the robustness of the results different filters were tested for many events.

6. Results

Examples of splitting measurements for teleseismic SKS- and local S-waves are shown in Figures 2 and 4. The SK(K)S-splitting results are listed in Table 1 and shown in Figures 5, 6 and 7. The individual splitting results are listed in the Supplementary Table 1. For the investigation of SKS-waves, around 40000 waveforms recorded at 52 stations were observed in total. Of those, 152 SK(K)S-splitting measurements (<1%) at 42 stations gave good results. We also documented 89 null results (non-split; see Supplementary Table 2). For the investigation of the local S-waves, around 2800 waveforms recorded at 50 stations were observed in total. Of those, 242 S-splitting measurements (~8%) at 42 stations gave good results.

Resolving multiple layers of anisotropy, dipping layers or further lateral heterogeneities requires good backazimuthal coverage of teleseismic events. Unfortunately, for the stations in this work this is not possible, as most teleseismic phases arrive from the north or west, a problem that has also been observed by other studies in the region (Piñero-Feliciangeli & Kendall, 2008; Meighan & Pulliam, 2013). As a consequence, we do not focus on backazimuthal patterns but instead use local events to help delineate layering in anisotropy. However, a collection of splitting data as a function of backazimuth at four stations can be found in the supplementary material.

6.1. Teleseismic SKS-splitting results

The polarisation direction of the fast shear-wave is mostly parallel to the trench. The mean value is 1.34±0.31 s for SK(K)S-measurements. The splitting results are independent of the filter boundaries, both in angle and delay time. General trench-parallel orientation has been observed in previous studies (Russo et al., 1996; Piñero Feliciangeli & Kendall, 2008; Benford et al., 2012; Meighan & Pulliam, 2013; Lynner and Long, 2013; Hodges & Miller, 2015). For many stations our results agree with previous results. Since our investigation was carried out uniformly for each station that gives us confidence in the results deviating from this trend.

In the remainder of the section we discuss anomalies to the trench-parallel pattern going from north to south. Additionally, we compare our findings to previous results where possible to either confirm the existing results or point out differences, searching for explanations.

6.1.1. Hispaniola

On the island of Hispaniola, stations SDD and PCDR show approximately trench-parallel alignment. This is in good agreement with results of Meighan & Pulliam (2013). At station SDD, located in the centre of the Hispaniola microplate, Benford et al. (2012) state that the number of observations of “Good and Fair splitting" results is low compared to other stations used in that study. They attribute the lack of measurements to the absence of anisotropy in this region as a result of locally undeformed mantle. However, despite having a large uncertainty, their result follows the trench-parallel alignment and agrees with our result in both delay time and orientation angle.

At station SMN1, which is located at the edge of the Hispaniola microplate, north of the eastern part of the Septentrional fault (Mann et al., 1998), our result, based on two events, shows a trench-perpendicular fast shear-wave polarisation. This is inconsistent with the result of Meighan & Pulliam (2013) who observe trench-parallel alignment also using two events. Without more data, it is not clear which result is correct.

6.1.2. Puerto Rico and Virgin Islands

The western stations on Puerto Rico (AGPR, AOPR, CRPR, ICM, MPR, OBIP) progressively show a clockwise rotation towards a trench-perpendicular orientation of the fast shear-wave. It should noted that even though two plates subduct beneath the Puerto Rico microplate from the north (North American plate) and from the south (Caribbean plate), the results are perpendicular to both trenches. This behaviour was not observed by Meighan & Pulliam (2013) or Hodges & Miller (2015). However, both studies find orientations at the northern stations (AGPR, AOPR, MPR) that divert from trench-parallel alignment in a rotation towards our results.

East of Puerto Rico at station STVI the stacked result shows a trench-parallel orientation. This agrees with Meighan & Pulliam (2013) and Hodges & Miller (2015) but is nearly orthogonal to the orientation seen by Benford et al. (2012). The latter work, though, stated an unusually high time lag with a high degree of uncertainty and scatter. Our individual results, albeit more numerous, seem to be more robust and mostly clustered around distinct values for φ (-58.0±1.8) and δt (1.13±0.02).

At station CDVI a trench-perpendicular orientation of the fast wave can be observed. This behaviour has been seen by Meighan & Pulliam (2013) but not by Hodges & Miller (2015). We do not observe a continuation of the trench-perpendicular orientation pattern to station ABVI in the north. This is based on a stack of three robust individual measurements.

6.1.3. Montserrat

On Montserrat the individual results show a large variety in shear-wave splitting angles. We therefore investigate the results stacking the stations individually as well (see Figure 7). On the five stations where Piñero Feliciangeli & Kendall (2008) observe splitting parameters the results are in very good agreement. Our combined stack is altered by five additional stations. Especially stations MBLY and MBWH deviate from the general pattern. The results were obtained correcting for the temporal misorientations of some of these stations (see Baird et al., 2015 for detail).

6.1.4. Martinique, St. Lucia and St. Vincent

The station FDF on Martinique has been active as part of the Geoscope network for a much longer time than the other Martinique stations that are part of the local observatory. Our splitting results show a counterclockwise rotation from trench-parallel alignment. While station ILAM in the north shows trench-parallel alignment, station MPOM in the south shows a strong trench-perpendicular trend. The result of station FDF indicates a transition from north to south, with the value of the orientation angle being between the values of the two other stations. Results for FDF from previous studies show this counterclockwise rotation as well.

Though station MPOM only provided one good splitting measurement, the observation is supported by results for next station to the south (MCLT on St. Lucia), which also shows a trench-perpendicular fast shear-wave polarisation. Even though only a few events were used at this station, the measurements are of high-quality and satisfy our criteria for a good measurement. This pattern has not been observed before.

At station SVB (St. Vincent) the fast shear-wave polarisation angle deviates from the trench-parallel orientation in a similar way as station FDF on Martinique, based on two events. This contradicts the result by Meighan & Pulliam (2013) who observed a trench-parallel pattern, based on two events as well, but with larger uncertainties both in orientation angle and delay time.

6.1.5. Barbados

The island of Barbados is not part of any volcanic arc, active or remnant. It is located a few tens of kilometres to the east and therefore does not experience any influence of the mantle wedge. Our result shows a clockwise rotation away from the trench-parallel orientation angle. This is significantly different from the trench-parallel orientation found by Meighan & Pulliam (2013). However, our results were obtained using more 'good' splitting measurements, combining SKS- and SKKS-measurements.

6.2. Local S-splitting results and comparison to the SKS results

The pattern observed by individual local S-splitting results is more complex (Figures 8 and 9). In contrast to the teleseismic core phases, stacking individual results is not possible, as the initial source polarisation will be variable. The horizontal component of the ray paths can be relatively large compared to the vertical components, and any part of the ray path may be anisotropic. Therefore, the results cannot be interpreted as point measurements beneath the receiver. Hence, the results are plotted at the straight-line midpoint of the ray path.

Individual results are combined using rose diagrams of subcells of the area. The rose diagrams show overall trends in the fast polarisation direction. In this work a mostly trench-parallel behaviour is observed in the NCPBZ and the northern part of the LAA (north of 15°N). In the rest of the LAA the pattern is more complicated, showing an increase in trench-perpendicular aligned results.

7. Interpretation

Two main questions are addressed in this section: a) At what depths are the regions of anisotropy located? b) What causes the observed behaviour in fast shear-wave polarisation?

To answer the first question a look at the change in delay time with depth provides useful hints (Figure 10). In all subcells the delay times from local events do not change with depth down to 200 km, suggesting most of the anisotropy seen by the local S-phases is in the crust. The delay times from teleseismic events are significantly larger. Therefore, the mantle wedge can be ruled out as a region of significant anisotropy. It is possible that a more complex anisotropic structure in the mantle wedge results in a destructive pattern. The main region of anisotropy has to be in the slab or beneath it.

To answer the second question we return to the potential explanations for mantle anisotropy in subduction regions, as presented in the introduction. Generally, a strong trench-parallel orientation can be observed in many teleseismic shear-wave splitting results. B-type olivine LPO cannot explain this behaviour. The mantle wedge beneath the LAA and the NCPBZ does not show anisotropy. Since our study uses local S-events from events above and below 80 to 90 km, we should see a change in fast-shear wave orientation (as shown in Kneller et al., 2005 or Karato et al., 2008), which is not the case. Furthermore, B-type olivine is not found to be dominant in the upper mantle beneath ocean basines (Zhang & Karato, 1995; Debayle et al., 2005). Due to the isotropic nature of the wedge we can also rule out a large abundance of serpentine with an aligned fabric in this region. Aligned serpentinised cracks in the subducting slab only works as an explanation in the serpentinite stability field (to depths of about 100 km; Ulmer & Trommsdorf, 1995) and has no effect at greater depths. Our splitting results do not show a transition in orientation angle or splitting magnitude at this depth. This does not rule out the serpentinised-crack model as a contributing mechanism, but it makes it impossible to be the primary cause. With our method it is not possible to rule out the entrainment of a sub-slab asthenosphere layer as a cause of the observed shear-wave splitting. However, it would show transitions in orientation of teleseismic S waves, depending on the steepness of the slab dip in combination with the incidence angle of the wave. In the Lesser Antilles this is not observed (Lynner & Long,2013) and is, therefore, unlikely.

This leaves two mechanisms to explain the trench-parallel orientation and the delay times. The anisotropic signal can originate from within the subducted slab, retained before the subduction by plate cooling, or from mantle flow around the subducting slab. 3D ray tracing models show a similar delay time and fast shear wave orientation for both. It is also possible to have a combination of the two mechanisms. Mantle flow was used as an interpretation in previous works (Piñero-Feliciangeli & Kendall, 2008; Lynner & Long, 2013; Meighan & Pulliam, 2013; Hodges & Miller, 2015). The near stationary Caribbean plate is wedged between subducting plates to the east and the west, and we are likely seeing the deflection of mantle material around this. However, we do see some notable deviations from slab-parallel orientations, which may indicate tears in the slabs of the LAA and NCPBZ.

Across the NCPBZ the results from teleseismic events show a large range in orientations, which indicates heterogeneous anisotropy beneath the island of Puerto Rico. This can be explained by the complex tectonic setting of the Puerto Rico microplate, located above two subduction zones. The complexity of this region was also discussed by Piñero-Feliciangeli & Kendall (2008) based on their results for station SJG on Puerto Rico.

Trench-perpendicular orientation can be observed at station CDVI, east of Puerto Rico. A slab tear accompanied by mantle flow through that gap (ten Brink, 2005) can explain this behaviour. This is likely to be a result of the Puerto Rico microplate rotation. Models for microplate rotation have been investigated before (McKenzie & Jackson, 1986) and the effect on mantle flow has been observed in regions such as Central America (Abt et al., 2010). In contrast to the results of Meighan & Pulliam (2013), a continuation of that orientation to the north cannot be observed. Instead it is possible that the location of the slab tear continues towards the northeast. Another influence of the microplate rotation on the mantle flow can be observed in northwestern Puerto Rico. There the fast shear-wave polarisations show a counterclockwise rotation towards trench-perpendicular orientations.

At the islands of Montserrat and Barbuda the main direction of shear-wave splitting orientations from local events is trench-perpendicular. This is also perpendicular to the trench-parallel alignment observed with splitting measurements from teleseismic events. There are some indications that the cause for these changes does not lie in the mantle wedge. First, a turn from trench-parallel to -perpendicular orientation can be caused by a change from B- to A-type olivine due to the drier mantle conditions. However, Schlaphorst et al. (2016) observed a higher amount of subducted water around this area with the subduction of the Fifteen-Twenty fracture zone. Results from that study consider a larger amount of water being subducted further south, around the island of Dominica, yet the local splitting results do not show a prominent deviation to a trench-parallel orientation around that island. Overall, the patchy pattern of subducted water does not show a similar pattern in local fast shear-wave splitting directions. Second, as stated before, the delay times are small and do not increase with depth (Figure 10). This fact alone leads to a conclusion that the region of anisotropy is to be found in the crust, a result proposed previously (Piñero-Feliciangeli & Kendall, 2008; Roman et al., 2011) and Baird et al. (2015). Furthermore, the results around Montserrat are of similar orientation and delay time to the ones at station ABVI. At that station the mantle wedge cannot be used as an explanation for the region of anisotropy, which strengthens the argument for crustal anisotropy. Since the SKS-splitting results do not show this pattern, we conclude that a second stronger anisotropic layer is present at a greater depth, driven by mantle flow beneath the slab, as concluded by Piñero-Feliciangeli & Kendall (2008) and Lynner & Long (2013).

Between the islands of Martinique, St. Lucia and St. Vincent the stations FDF, MCLT, MPOM and SVB show trench-perpendicular fast shear-wave polarisations. This behaviour can be explained by mantle flow through a tear in the subducting slab. Based on numerical modelling Gerya et al. (2015) show that vertical tears can easily form in curved subduction zones. Since in our case the location also coincides with the subduction of a fracture zone (Schlaphorst et al., 2016), a segmentation of the subduction zone is possible (Rosenbaum et al., 2008). In this case it is consistent with the proposed boundary between the North and South American plates (Benthem et al., 2013). Wadge & Shepherd (1984) observe a change in the orientation and the dip of the Wadati-Benioff zone in the area between Martinique and St. Lucia introducing the idea of a slab gap. On St. Vincent our result contradicts the result by Meighan & Pulliam (2013). Both studies stack two events but in our study the uncertainties in orientation angle of the fast wave and in delay time are smaller.

In the south, around the islands of Grenada and Tobago our results show a trench-parallel orientation of the fast shear-wave, which contradicts the results of Lynner & Long (2013) who use source-side splitting to estimate the anisotropy. Their observed pattern of alignment with the motion of the South American plate is interpreted to be a result of the blocking of a southward mantle flow by the thick continental root. They conclude that trench-perpendicular stretching due to the migration of the slab could explain the observed pattern in the south. Our results and the results of Meighan & Pulliam (2013) use direct observations from core phases recorded at stations on these islands and do not see this behaviour. However, further to the south in Trinidad and northern Venezuela Russo et al. (1996) find orientations parallel to those observed by Lynner & Long (2013). A further investigation of the area between the southern end of the LAA and the northeastern part of South America is needed to constrain the mantle flow in this region, but at face value our results suggest uninterrupted trench-parallel mantle flow beneath the subducting slab.

Alvarez (1982, 2001) has argued that the Caribbean is one of the regions, where sub lithospheric mantle flow from the Pacific to the Atlantic compensates for the shrinking of the Pacific. Interestingly our results reveal deviations from trench mantle flow in the regions proposed by this model. One of these regions also agrees with a proposed location of the boundary between the North American and South American plates.

8. Conclusions

In this work we investigated seismic anisotropy in the subduction environment of the LAA and the NCPBZ using shear-wave splitting measurements on teleseismic and local events recorded at 52 island stations across that region. To date, this is the most comprehensive dataset used to study crust and mantle anisotropy in this region. These results were used to infer deformation structures in the mantle across this complicated plate boundary. Shear-wave splitting in teleseismic core phases shows a broadly trench parallel fast shear-wave polarisation along the LAA and NCPBZ. This agrees with the interpretation of continuous trench-parallel mantle flow proposed by Piñero-Feliciangeli & Kendall (2008) and Lynner & Long (2013), which is due to the subducting slab acting as a barrier to mantle flow beneath the Caribbean and North/South American plates.

Shear-wave splitting measured in local S-phases with depths down to 200 km suggest that the upper mantle wedge beneath the Caribbean in this region is isotropic and that most of the anisotropy observed by these phases is confined to the crust. These observations agree with previous observations, which were albeit described at fewer stations and suggest that splitting in teleseismic phases is primarily sensitive to anisotropy within or below the slab.

However, there are a number of measurements that show significant deviations from the slab parallel orientations in mantle anisotropy. Two anomalies are observed beneath the NCPBZ. We map a sharp change to a trench-perpendicular orientation east of Puerto Rico. This anomaly can be explained by mantle flow through a slab tear, as previously proposed by ten Brink (2005) and based on seismicity patterns. Our results suggest that this tear trends towards the east, which is a slightly different interpretation from Meighan & Pulliam (2013), who argue the tear extends in a more northerly direction. This is primarily based on our analysis of more data and different results observed at station ABVI. A second anomaly, not previously observed, is a trench-perpendicular pattern at stations in western Puerto Rico. This can be explained by the counterclockwise rotation of Puerto Rico and the ongoing opening of the Mona Passage (Dolan et al., 1998). Hence, it would appear that there are at least two potential slab windows where mantle can flow across the subducting slabs of the NCPBZ.

There is a clear deviation from slab-parallel flow beneath the LAA between Martinique and St. Vincent. This is visible in core-phase splitting at four stations. Again, this pattern can be explained by a mantle flow through a gap in the subducting plate. Wadge & Shepherd (1984) observe a vertical gap in the Wadati-Benioff zone in this region using a seismicity catalogue from local seismic networks. This feature has been also proposed for this area based on tomographic models (Benthem et al., 2013). Our observations further strengthen the argument that the plate boundary between the North and South American plates lies in this region.

The gaps in both the LAA and the NCPBZ agree with previously proposed gaps in the slabs of the eastern Caribbean, which allow eastward sublithospheric mantle flow in response to the shrinking of the Pacific plate (Alvarez 1982; 2001). A detailed study of the area using a denser array of seismic stations, including ocean bottom seismometers, would help to investigate these features further.

Acknowledgements

The authors would like to thank the British Geological Survey (BGS), the Seismic Research Centre of The University of the West Indies (SRC), and the Institut de Physique du Globe de Paris (IPGP) for providing the data used in this study. Partial funding for this project comes from the BGS and a grant from the Natural Environment Research Council (NERC – NE/K004328/1). The authors would like to thank Andréa Tommasi and an anonymous reviewer for their constructive and helpful feedback.

References

Abt, D.L., Fischer, K.M., Abers, G.A., Protti, M., González, V. and Strauch, W., 2010. Constraints on upper mantle anisotropy surrounding the Cocos slab from SK (K) S splitting. *Journal of Geophysical Research: Solid Earth*, *115*(B6), doi: 10.1029/2009JB006710.

Al-Harrasi, O.H., Kendall, J.M. and Chapman, M., 2011. Fracture characterization using frequency-dependent shear wave anisotropy analysis of microseismic data. *Geophysical Journal International*, *185*(2), pp.1059-1070, doi: 10.1111/j.1365-246X.2011.04997.x.

Alsina, D. and Snieder, R., 1995. Small-scale sublithospheric continental mantle deformation: constraints from SKS splitting observations. *Geophysical Journal International*, *123*(2), pp.431-448, doi: 10.1111/j.1365-246X.1995.tb06864.x.

Alvarez, W., 1982. Geological evidence for the geographical pattern of mantle return flow and the driving mechanism of plate tectonics. *Journal of Geophysical Research: Solid Earth*, *87*(B8), pp.6697-6710, doi: 10.1029/JB087iB08p06697.

Alvarez, W., 2001. Eastbound sublithosphere mantle flow through the Caribbean gap and its relevance to the continental undertow hypothesis. *Terra Nova*, *13*(5), pp.333-337, doi: 10.1046/j.1365-3121.2001.00356.x.

Backus, G.E., 1962. Long-wave elastic anisotropy produced by horizontal layering. *Journal of Geophysical Research*, *67*(11), pp.4427-4440, doi: 10.1029/JZ067i011p04427.

Baird, A.F., Kendall, J.M., Sparks, R.S.J. and Baptie, B., 2015. Transtensional deformation of Montserrat revealed by shear wave splitting. *Earth and Planetary Science Letters*, *425*, pp.179-186, doi: 10.1111/j.1365-246X.2009.04414.x.

Benford, B., Tikoff, B. and DeMets, C., 2012. Character of the Caribbean–Gônave–North America plate boundaries in the upper mantle based on shear-wave splitting. *Geophysical Research Letters*, *39*(24), doi: 10.1029/2012GL053766.

Benthem, S., Govers, R., Spakman, W. and Wortel, R., 2013. Tectonic evolution and mantle structure of the Caribbean. *Journal of Geophysical Research: Solid Earth*, *118*(6), pp.3019-3036, doi: 10.1002/jgrb.50235.

Bird, P., 2003. An updated digital model of plate boundaries. *Geochemistry, Geophysics, Geosystems*, *4*(3), doi: 10.1029/2001GC000252.

Bouysse, P., 1988. Opening of the Grenada back-arc basin and evolution of the Caribbean Plate during the Mesozoic and early Paleogene. *Tectonophysics*, *149*(1), pp.121-143, doi: 10.1016/0040-1951(88)90122-9.

Bouysse, P., Westercamp, D. and Andreieff, P., 1990. 4. The Lesser Antilles Island Arc. In *Proceedings of the Ocean Drilling Program: Scientific results* (Vol. 110, p. 29). The Program.

Christeson, G.L., Mann, P., Escalona, A. and Aitken, T.J., 2008. Crustal structure of the Caribbean–northeastern South America arc-continent collision zone. *Journal of Geophysical Research: Solid Earth*, *113*(B8), doi: 10.1029/2007JB005373.

Crampin, S., McGonigle, R. and Bamford, D., 1980. Estimating crack parameters from observations of P-wave velocity anisotropy. *Geophysics*, *45*(3), pp.345-360, doi: 10.1190/1.1441086.

Crampin, S., Evans, R., Üçer, B., Doyle, M., Davis, J.P., Yegorkina, G.V. and Miller, A., 1980. Observations of dilatancy-induced polarization anomalies and earthquake prediction. *Nature*, *286*(5776), pp.874-877.

Debayle, E., Kennett, B. and Priestley, K., 2005. Global azimuthal seismic anisotropy and the unique plate-motion deformation of Australia. *Nature, 433*(7025), pp.509-512, doi: 10.1038/nature03247.

Di Leo, J.F., Wookey, J., Hammond, J.O.S., Kendall, J.M., Kaneshima, S., Inoue, H., Yamashina, T. and Harjadi, P., 2012. Deformation and mantle flow beneath the Sangihe subduction zone from seismic anisotropy. *Physics of the Earth and Planetary Interiors*, *194*, pp.38-54, doi: 10.1016/j.pepi.2012.01.008.

Dolan, J.F., Mullins, H.T. and Wald, D.J., 1998. Active tectonics of the north-central Caribbean: Oblique collision, strain partitioning, and opposing subducted slabs. *SPECIAL PAPERS-GEOLOGICAL SOCIETY OF AMERICA*, pp.1-62.

Evans, R., 1984. Effects of the free surface on shear wavetrains. *Geophysical Journal International*, *76*(1), pp.165-172, doi: 10.1111/j.1365-246X.1984.tb05032.x.

Faccenda, M., Burlini, L., Gerya, T.V. and Mainprice, D., 2008. Fault-induced seismic anisotropy by hydration in subducting oceanic plates. *Nature*, *455*(7216), pp.1097-1100, doi: 10.1038/nature07376.

Gerya, T.V., Stern, R.J., Baes, M., Sobolev, S.V. and Whattam, S.A., 2015. Plate tectonics on the Earth triggered by plume-induced subduction initiation. *Nature*, *527*(7577), pp.221-225, doi: 10.1038/nature15752.

Haberland, C. and Rietbrock, A., 2001. Attenuation tomography in the western central Andes: A detailed insight into the structure of a magmatic arc. *Journal of Geophysical Research: Solid Earth*, *106*(B6), pp.11151-11167, doi: 10.1029/2000JB900472.

Hall, C.E., Fischer, K.M., Parmentier, E.M. and Blackman, D.K., 2000. The influence of plate motions on three-dimensional back arc mantle flow and shear wave splitting. *Journal of Geophysical Research: Solid Earth*, *105*(B12), pp.28009-28033, doi: 10.1029/2000JB900297.

Hall, S.A., Kendall, J.M. and van der Baan, M., 2004. Some comments on the effects of lower-mantle anisotropy on SKS and SKKS phases. *Physics of the Earth and Planetary Interiors*, *146*(3), pp.469-481, doi: 10.1016/j.pepi.2004.05.002.

Hammond, J.O.S., Kendall, J.M., Angus, D. and Wookey, J., 2010. Interpreting spatial variations in anisotropy: insights into the Main Ethiopian Rift from SKS waveform modelling. *Geophysical Journal International*, *181*(3), pp.1701-1712, doi: 10.1111/j.1365-246X.2010.04587.x.

Healy, D., Reddy, S.M., Timms, N.E., Gray, E.M. and Brovarone, A.V., 2009. Trench-parallel fast axes of seismic anisotropy due to fluid-filled cracks in subducting slabs. *Earth and Planetary Science Letters*, *283*(1), pp.75-86, doi: 10.1016/j.epsl.2009.03.037.

Jung, H. and Karato, S.I., 2001. Water-induced fabric transitions in olivine. *Science*, *293*(5534), pp.1460-1463, 10.1126/science.1062235.

Jung, H., Mo, W. and Green, H.W., 2009. Upper mantle seismic anisotropy resulting from pressure-induced slip transition in olivine. *Nature Geoscience*, *2*(1), pp.73-77, doi: 10.1038/ngeo389.

Karato, S.I., Jung, H., Katayama, I. and Skemer, P., 2008. Geodynamic significance of seismic anisotropy of the upper mantle: new insights from laboratory studies. *Annu. Rev. Earth Planet. Sci.*, 36, pp.59-95, doi: 10.1146/annurev.earth.36.031207.124120.

Katayama, I., Hirauchi, K.I., Michibayashi, K. and Ando, J.I., 2009. Trench-parallel anisotropy produced by serpentine deformation in the hydrated mantle wedge. *Nature*, *461*(7267), pp.1114-1117, doi: 10.1038/nature08513.

Keir, D., Kendall, J.M., Ebinger, C.J. and Stuart, G.W., 2005. Variations in late syn-rift melt alignment inferred from shear-wave splitting in crustal earthquakes beneath the Ethiopian rift. *Geophysical Research Letters*, *32*(23), doi: 10.1029/2005GL024150.

Kendall, J.M., 2000. Seismic anisotropy in the boundary layers of the mantle. *Earth's Deep Interior: Mineral physics and tomography from the atomic to the global scale*, pp.133-159, doi: 10.1029/GM117p0133.

Kneller, E.A., Van Keken, P.E., Karato, S.I. and Park, J., 2005. B-type olivine fabric in the mantle wedge: insights from high-resolution non-Newtonian subduction zone models. *Earth and Planetary Science Letters*, *237*(3), pp.781-797, doi: 10.1016/j.epsl.2005.06.049.

Lin, J.Y., Hsu, S.K. and Sibuet, J.C., 2004. Melting features along the Ryukyu slab tear, beneath the southwestern Okinawa Trough. *Geophysical research letters*, *31*(19), doi: 10.1029/2004GL020862.

Long, M.D. and van der Hilst, R.D., 2006. Shear wave splitting from local events beneath the Ryukyu arc: trench-parallel anisotropy in the mantle wedge. *Physics of the earth and planetary interiors*, *155*(3), pp.300-312, doi: 10.1016/j.pepi.2006.01.003.

Long, M.D. and Silver, P.G., 2008. The subduction zone flow field from seismic anisotropy: A global view. *Science*, *319*(5861), pp.315-318, doi: 10.1126/science.1150809.

Long, M.D. and Silver, P.G., 2009. Mantle flow in subduction systems: The subslab flow field and implications for mantle dynamics. *Journal of Geophysical Research: Solid Earth*, *114*(B10), doi: 10.1029/2008JB006200.

Lowman, J.P., Pinero-Feliciangeli, L.T., Kendall, J. and Shahnas, M.H., 2007. Influence of convergent plate boundaries on upper mantle flow and implications for seismic anisotropy. *Geochemistry, Geophysics, Geosystems*, *8*(8), doi: 10.1029/2007GC001627.

Lynner, C. and Long, M.D., 2013. Sub-slab seismic anisotropy and mantle flow beneath the Caribbean and Scotia subduction zones: Effects of slab morphology and kinematics. *Earth and Planetary Science Letters*, *361*, pp.367-378, doi: 10.1016/j.epsl.2012.11.007.

Mainprice, D. and Nicolas, A., 1989. Development of shape and lattice preferred orientations: application to the seismic anisotropy of the lower crust. *Journal of Structural Geology*, *11*(1-2), pp.175-189, doi: 10.1016/0191-8141(89)90042-4.

Masson, D.G. and Scanlon, K.M., 1991. The neotectonic setting of Puerto Rico. *Geological Society of America Bulletin*, *103*(1), pp.144-154, doi: 10.1130/0016-7606(1991)103<0144:TNSOPR>2.3.CO;2.

Mazzotti, S., Henry, P., LePichon, X. and Sagiya, T., 1999. Strain partitioning in the zone of transition from Nankai subduction to Izu–Bonin collision (Central Japan): implications for an extensional tear within the subducting slab. *Earth and planetary science letters*, *172*(1), pp.1-10, doi: 10.1016/S0012-821X(99)00189-2.

McKenzie, D. and Jackson, J., 1986. A block model of distributed deformation by faulting. *Journal of the Geological Society*, *143*(2), pp.349-353, doi: 10.1144/gsjgs.143.2.0349.

Meighan, H.E. and Pulliam, J., 2013. Seismic anisotropy beneath the northeastern Caribbean: implications for the subducting North American lithosphere. *Bulletin de la Société Géologique de France*, *184*(1-2), pp.67-76, doi: 10.2113/gssgfbull.184.1-2.67.

Meighan, H.E., Pulliam, J., Brink, U. and López-Venegas, A.M., 2013. Seismic evidence for a slab tear at the Puerto Rico Trench. *Journal of Geophysical Research: Solid Earth*, *118*(6), pp.2915-2923, doi: 10.1002/jgrb.50227.

Müller, R.D. and Smith, W.H., 1993. Deformation of the oceanic crust between the North American and South American plates. *Journal of Geophysical Research: Solid Earth*, *98*(B5), pp.8275-8291, doi: 10.1029/92JB02863.

Piñero-Feliciangeli, L.T. and Kendall, J.M., 2008. Sub-slab mantle flow parallel to the Caribbean plate boundaries: Inferences from SKS splitting. *Tectonophysics*, *462*(1), pp.22-34, doi: 10.1016/j.tecto.2008.01.022.

Restivo, A. and Helffrich, G., 1999. Teleseismic shear wave splitting measurements in noisy environments. *Geophysical Journal International*, *137*(3), pp.821-830, doi: 10.1046/j.1365-246x.1999.00845.x.

Ribe, N.M., 1989. Seismic anisotropy and mantle flow. *Journal of Geophysical Research: Solid Earth*, *94*(B4), pp.4213-4223, doi: 10.1029/JB094iB04p04213.

Rosenbaum, G., Gasparon, M., Lucente, F.P., Peccerillo, A. and Miller, M.S., 2008. Kinematics of slab tear faults during subduction segmentation and implications for Italian magmatism. *Tectonics*, *27*(2), doi: 10.1029/2007TC002143.

Russo, R.M. and Silver, P.G., 1994. Trench-parallel flow beneath the Nazca plate from seismic anisotropy. *Science*, pp.1105-1105.

Russo, R.M., Silver, P.G., Franke, M., Ambeh, W.B. and James, D.E., 1996. Shear-wave splitting in northeast Venezuela, Trinidad, and the eastern Caribbean. *Physics of the Earth and Planetary Interiors*, *95*(3), pp.251-275, doi: 10.1016/0031-9201(95)03128-6.

Savage, M.K., 1999. Seismic anisotropy and mantle deformation: what have we learned from shear wave splitting?. *Reviews of Geophysics*, *37*(1), pp.65-106, doi: 10.1029/98RG02075.

Savage, M.K. and Silver, P.G., 1993. Mantle deformation and tectonics: constraints from seismic anisotropy in the western United States. *Physics of the Earth and Planetary Interiors*, *78*(3-4), pp.207-227, doi: 10.1016/0031-9201(93)90156-4.

Schlaphorst, D., Kendall, J.M., Collier, J.S., Verdon, J.P., Blundy, J., Baptie, B., Latchman, J.L., Massin, F. and Bouin, M.P., 2016. Water, oceanic fracture zones and the lubrication of subducting plate boundaries—insights from seismicity. *Geophysical Journal International*, *204*(3), pp.1405-1420, doi: 10.1093/gji/ggv509.

Silver, P.G., 1996. Seismic anisotropy beneath the continents: Probing the depths of geology. *Annual review of earth and planetary sciences*, *24*, pp.385-432.

Silver, P.G. and Chan, W.W., 1991. Shear wave splitting and subcontinental mantle deformation. *Journal of Geophysical Research: Solid Earth*, *96*(B10), pp.16429-16454, doi: 10.1029/91JB00899.

Silver, P.G. and Savage, M.K., 1994. The interpretation of shear-wave splitting parameters in the presence of two anisotropic layers. *Geophysical Journal International*, *119*(3), pp.949-963, doi: 10.1111/j.1365-246X.1994.tb04027.x.

Song, T.R.A. and Kawakatsu, H., 2012. Subduction of oceanic asthenosphere: evidence from sub-slab seismic anisotropy. *Geophysical Research Letters*, *39*(17), doi: 10.1029/2012GL052639.

Stein, S., Engeln, J.F., Wiens, D.A., Fujita, K. and Speed, R.C., 1982. Subduction seismicity and tectonics in the Lesser Antilles arc. *Journal of*

Geophysical Research: Solid Earth, *87*(B10), pp.8642-8664, doi: 10.1029/JB087iB10p08642.

Teanby, N.A., Kendall, J.M. and Van der Baan, M., 2004. Automation of shear-wave splitting measurements using cluster analysis. *Bulletin of the Seismological Society of America*, *94*(2), pp.453-463, doi: 10.1785/0120030123.

Ten Brink, U., 2005. Vertical motions of the Puerto Rico Trench and Puerto Rico and their cause. *Journal of Geophysical Research: Solid Earth*, *110*(B6), doi: 10.1029/2004JB003459.

Tomblin, J.F., 1975. The Lesser Antilles and Aves Ridge. In *The Gulf of Mexico and the Caribbean* (pp. 467-500). Springer US, doi: 10.1007/978-1-4684-8535-6_11.

Ulmer, P. and Trommsdorff, V., 1995. Serpentine stability to mantle depths and subduction-related magmatism. Science, 268(5212), p.858, doi: 10.1126/science.268.5212.858.

VanDecar, J.C., Russo, R.M., James, D.E., Ambeh, W.B. and Franke, M., 2003. Aseismic continuation of the Lesser Antilles slab beneath continental South America. *Journal of Geophysical Research: Solid Earth*, *108*(B1), doi: 10.1029/2001JB000884.

Wadge, G. and Shepherd, J.B., 1984. Segmentation of the Lesser Antilles subduction zone. *Earth and Planetary Science Letters*, *71*(2), pp.297-304, doi: 10.1016/0012-821X(84)90094-3.

Webb, S.C., 1991, October. Measurements of the wavenumber-frequency spectrum of oceanic microseisms. In *OCEANS'91. Ocean Technologies and Opportunities in the Pacific for the 90's. Proceedings.* (Vol. 1, pp. 102-106). IEEE, doi: 10.1109/OCEANS.1991.627916.

Westbrook, G.K., 1975. The structure of the crust and upper mantle in the region of Barbados and the Lesser Antilles. *Geophysical Journal International*, *43*(1), pp.201-242, doi: 10.1111/j.1365-246X.1975.tb00632.x.

Westbrook, G.K., Mascle, A. and Biju-Duval, B., 1984. 2. GEOPHYSICS AND THE STRUCTURE OF THE LESSER ANTILLES FOREARC1. *Biju-Duval et al., Initial Reports of DSDP, LXXVIII, US Government Printing Office, Washington, DC*, pp.23-38.

Wolfe, C.J. and Silver, P.G., 1998. Seismic anisotropy of oceanic upper mantle: Shear wave splitting methodologies and observations. *Journal of Geophysical Research: Solid Earth*, *103*(B1), pp.749-771, doi: 10.1029/97JB02023.

Wookey, J., 2012. Direct probabilistic inversion of shear wave data for seismic anisotropy. *Geophysical Journal International*, *189*(2), pp.1025-1037, doi: 10.1111/j.1365-246X.2012.05405.x.

Zhang, S. and Karato, S.I., 1995. Lattice preferred orientation of olivine aggregates deformed in simple shear. *Nature, 375*(6534), pp.774-777, doi: 10.1038/375774a0.

Tables:

Table 1: SKS-splitting results for each individual station with at least one measurement, including results from previous results. Note that Benford et al. (2012) and Hodges & Miller (2015) only show average results including individual results with an assigned quality of "fair", whereas the other studies use only "good" results.

Station	No.[1]	*φ±Δφ*	*δt±Δδt*	*Source*
ABD	2	-26.0±3.5	2.08±0.52	
ABVI	3	87.0±7.0	1.58±0.08	
	1	8.3±26.0	0.75±0.45	Meighan & Pulliam, 2013
	19	-66.7±7.9	1.9±0.74	Hodges & Miller, 2015
AGPR	2	-27.0±3.3	0.59±0.05	
	2	-63.7±11.8	1.1±0.45	Meighan & Pulliam, 2013
	7	-79.29±15.68	1.31±0.92	Hodges & Miller, 2015
ANWB	6	-65.0±4.3	1.20±0.08	
	5	-47.5±12.3	1.4±0.37	Benford et al., 2012
	25	-64.5±29.3	1.52±1.04	Meighan & Pulliam, 2013
	24	-55.6±23.0	1.38±0.66	Hodges & Miller, 2015
AOPR	16	-31.0±3.8	0.73±0.08	
	3	-75.8±17.2	1.55±0.62	Meighan & Pulliam, 2013
	29	-67.9±14.8	0.92±0.16	Hodges & Miller, 2015
BARV	16	84±2	2.1±0.2	Russo et al., 1996
BBGH	6	64.0±2.3	1.10±0.09	
	2	5.1±14.0	0.9±0.35	Meighan & Pulliam, 2013
CBYP	1	-80.0±7.5	2.17±0.15	
	3	-85±22.8	0.7±0.83	Meighan & Pulliam, 2013
	8	-35.8±17.5	0.51±0.20	Hodges & Miller, 2015
CDVI	1	22.0±7.8	2.00±0.11	
	2	37.5±27.5	0.75±0.53	Meighan & Pulliam, 2013
	10	-74.4±20.5	0.975±0.22	Hodges & Miller, 2015
CPD	4	-82.0±3.5	1.05±0.05	
CRPR[2]	2	-62.0±7.0	1.33±0.23	
DLPL	2	-3.0±18.5	1.13±0.29	
	2	3.5±26.3	1.8±0.53	Meighan & Pulliam, 2013
DSD	2	-60.0±4.0	1.13±0.05	
EMPR	5	-89±28.15	1.82±1.22	Hodges & Miller, 2015
FDF	3	-59.0±8.8	0.90±0.06	
	7	-43.6±16.6	1.19±0.63	Piñero-Feliciangeli & Kendall, 2008
	3	-39.4±9.2	1±0.48	Meighan & Pulliam, 2013
GRGR	2	66.0±3.3	1.73±0.13	
	2	41.5±16.3	2.6±0.53	Meighan & Pulliam, 2013
HUMP	3	-49.0±5.5	0.68±0.09	
	3	83.9±4.7	2.85±0.25	Meighan & Pulliam, 2013
	13	81.7±0.46	1.56±0.56	Hodges & Miller, 2015
ICM	1	-71.0±1.0	1.70±0.03	
ILAM	1	-3.0±20.8	0.77±0.70	
MVO[3]	23	-23.0±1.5	1.03±0.06	
	11	-41.1±7.4	1.68±0.28	Piñero-Feliciangeli & Kendall, 2008

MBBE	2	-24.0±4.3	1.05±0.22	
	1	-20.0±10.0	2.10±0.60	Piñero-Feliciangeli & Kendall, 2008
MBBY	2	-13.0±2.3	1.25±0.23	
	2	-18.5±10.0	1.93±0.42	Piñero-Feliciangeli & Kendall, 2008
MBFR	2	-32.0±4.5	1.13±0.14	
MBGA	1	-30.0±6.5	1.75±0.25	
MBGB	4	-37.0±6.5	0.80±0.14	
	4	-39.2±12.3	1.35±0.58	Piñero-Feliciangeli & Kendall, 2008
MBGH	4	-33.0±2.8	0.95±0.09	
	3	-39.2±16.33	1.31±1.38	Piñero-Feliciangeli & Kendall, 2008
MBLG	3	-30.0±6.5	2.03±0.16	
MBLY	1	-82.0±21.5	0.97±0.61	
MBRY	4	-22.0±3.0	1.15±0.11	
	1	-25.0±10.0	1.95±0.45	Piñero-Feliciangeli & Kendall, 2008
MBWH	1	-84.0±24.8	1.80±0.91	
MCLT	3	-68.0±12.5	0.65±0.09	
MGP[2]	2	-64.9±17.8	0.8±0.25	Meighan & Pulliam, 2013
	3	82.33±3.51	1.867±0.75	Hodges & Miller, 2015
MLPR	3	-82.25±9.7	1.68±0.54	Hodges & Miller, 2015
MPOM	1	-81.0±8.8	2.40±0.20	
MPR	1	-31.0±15.3	1.23±0.41	
	4	-65.7±10.0	1.3±0.39	Meighan & Pulliam, 2013
	8	-73±10.89	1.56±0.53	Hodges & Miller, 2015
MTP	1	-57.0±3.8	1.53±0.09	
	2	-83.9±6.5	2.1±0.43	Meighan & Pulliam, 2013
	6	-89.667	2.4±0.41	Hodges & Miller, 2015
OBIP	4	-48.0±5.0	0.90±0.14	
	3	-64.9±18.2	0.5±0.30	Meighan & Pulliam, 2013
	15	-86.3±11.2	1.14±0.27	Hodges & Miller, 2015
PCDR	1	-59.0±1.3	1.33±0.08	
	2	-49.8±13.5	2.1±0.38	Meighan & Pulliam, 2013
	7	-77.14±9.04	1.47±0.29	Hodges & Miller, 2015
PUCM[4]	3	-77.9±18.7	1.36±0.35	Meighan & Pulliam, 2013
RSLV	20	86±3	1.9±0.3	Russo et al., 1996
SABA	6	-58.0±4.5	1.10±0.06	
	5	-77.9±20.2	0.9±0.38	Meighan & Pulliam, 2013
	13	-64.3±3.0	1.18±0.05	Hodges & Miller, 2015
SDD	1	-57.0±3.3	1.33±0.18	
	3	-33.0±37.1	1.35±1.43	Benford et al., 2012
	2	-71.9±26.8	0.95±0.45	Meighan & Pulliam, 2013
SEUS	6	-44.0±7.0	0.98±0.13	
	2	-60.8±21.3	0.9±0.33	Meighan & Pulliam, 2013
	8	-60.4±10.0	1.03±0.22	Hodges & Miller, 2015
SJG	21	-84.0±2.8	0.83±0.04	
	13	85±1	1.2±0.2	Russo et al., 1996
	20	-89.3±9.0	1.29±0.27	Piñero-Feliciangeli & Kendall, 2008
	10	-78.6±20.9	1.23±1.10	Benford et al., 2012
	11	-87.63±15.4	1.24±0.55	Hodges & Miller, 2015
SMN1	2	30.0±3.5	1.78±0.21	
	2	-55.6±11.0	1.85±0.65	Meighan & Pulliam, 2013
SMRT	3	-67.0±4.3	1.20±0.11	
	3	-78.9±21.7	1±0.47	Meighan & Pulliam, 2013
	5	-79.1±17.3	1.13±0.06	Hodges & Miller, 2015
STVI	14	-58.0±1.8	1.13±0.02	

	6	61.0±54.2	2.89±1.23	Benford et al., 2012
	3	-81.9±5.0	2.35±0.28	Meighan & Pulliam, 2013
	10	-62.8±14.8	1.47±0.39	Hodges & Miller, 2015
SVB	2	-32.0±6.25	1.43±0.23	
	2	23.6±17.5	1.2±0.63	Meighan & Pulliam, 2013
TDBA	3	-31.0±2.3	1.40±0.24	
TOSP	1	24.0±5.3	0.85±0.07	
TRNV	13	95±11	1.9±0.2	Russo et al., 1996

[1] Number of stacked events.

[2] The location of stations CRPR and MGP are approximately 2 km apart. Results of both stations have been compared.

[3] Stack of 10 stations on Montserrat. The individual station results are listed as well. No SKS splitting results were found for MBGE and MBHA.

[4] Station PUCM is west of the area shown in figure 5.

Figures:

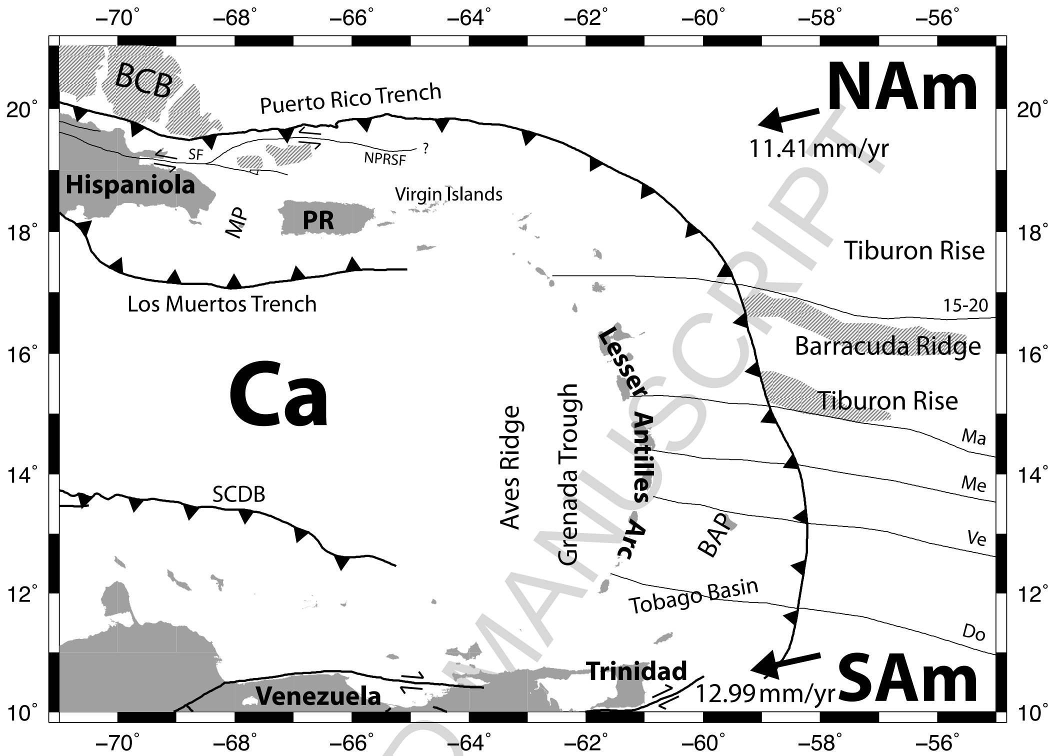

Figure 1: Structural map of the Eastern Caribbean. Landmasses are shown in grey. The plate names are abbreviated: Ca denotes the Caribbean, NAm the North American and SAm the South American plate. The northwest of the map shows the complex subduction environment of the Northern Caribbean Plate Boundary Zone (NCPBZ). The locations of the Bahamas Carbonate Banks (BCB), the island of Puerto Rico (PR) and the Mona Passage (MP), as well as the Septentrional Fault (SF) and the North Puerto Rico Slope Fault (NPSRF) are shown. Details are taken from Dolan et al. (1998). Towards the south the Southern Caribbean Deformed Belt (SCDB) marks the subduction of the Caribbean beneath the South American plate. In the east the five major fracture zones that originate at the Mid-Atlantic Ridge are shown (15-20: Fifteen-Twenty; Ma: Marathon; Me: Mercurius; Ve: Vema; Do: Doldrums). The Bahamas accretionary prism (BAP) is located around the island of Barbados. The plate motions of the North and South American plates are indicated by black arrows. Their length and angle indicate the motion and velocity of subduction relative to the Caribbean plate (DeMets et al., 2000).

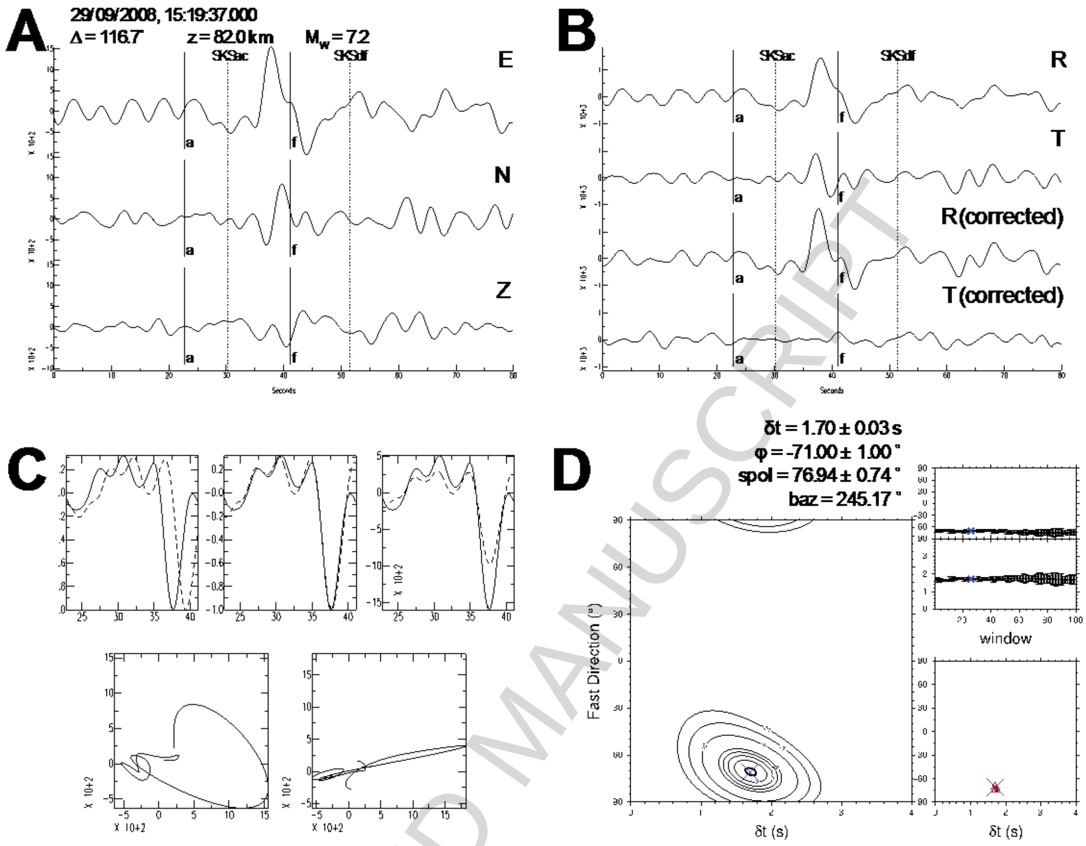

Figure 2: Example of an SKS-splitting measurement at station ICM (Puerto Rico) on a magnitude 7.2 event recorded on 29/09/2008, 15:19:37.000. The event originated at the Kermadec trench in the Pacific Ocean (29.80°S, 177.67° W, distance: 116.7°) at a depth of 82.0 km. A) The filtered (0.01–0.4 Hz) east-west (E), north-south (N) and vertical (Z) components. The solid vertical bars indicate the start (a) and end time (f) of the window used to isolate the SKS-wave. Note that 100 different windows were tested and this one gave the best result. The dashed vertical bars indicate theoretical arrival times of different phases, calculated using the *iasp91* reference model (Kennett & Engdahl, 1991). B) Radial (R) and transverse (T) components before and after the correction. For a good splitting measurement the energy on the transverse component should be minimised after the splitting correction. C) Top row: Fast (solid line) and slow (dashed line) shear-waves before (left) and after correction (middle and right). The amplitudes are normalised in the left and middle diagrams, true amplitudes are shown in the right panel. Bottom row: Particle motion in the polarisation plane within the defined window before (left) and after correction (right). Shear-wave splitting tends to an elliptical particle motion, which should be linearised

after the correction is applied. D) Big panel: Contour plot of the grid-search over δt and φ showing the second eigenvalue of the covariance matrix. The best splitting parameters are indicated by the cross, the thicker black line indicates the 95% confidence contour of the F test. Above the panel information about the splitting parameters (δt and φ), the source polarisation (spol) and the backazimuth (baz) is shown. Note that the source polarisation is less than 20° deviant from the opposite of the backazimuth. Small panels: Best splitting solutions for the 100 time windows around SKS (top) and cluster analysis of the solutions (bottom). A good result will be stable over different time windows, creating plateaus in both splitting parameters, with the best solutions clustering in one area. In this case the plateau spans the entire range of windows and all solutions cluster in one area.

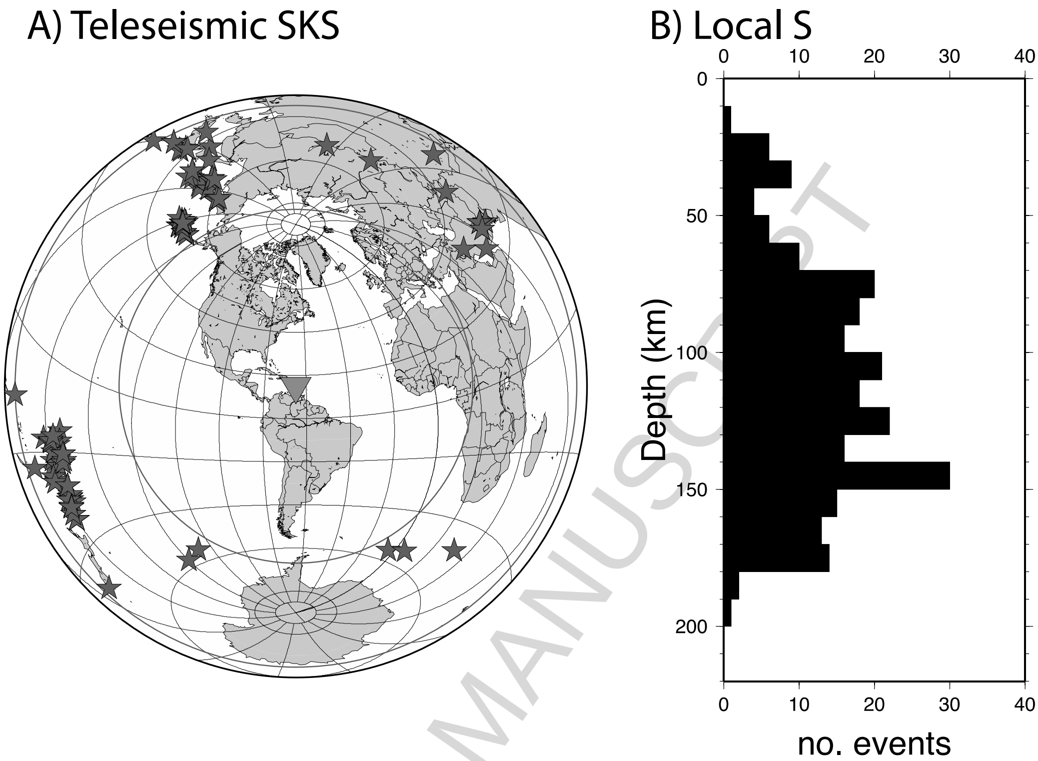

Figure 3: Teleseismic event locations and depths of local events. A) Azimuthal equidistant map showing the event locations of all teleseismic events used in this study (red stars). The red concentric circles represent the search distance of 85˚ to 135˚ (purple inverted triangle). Note that this is a combined plot for all stations using an average station position of 15˚N, 65˚W. B) Histogram showing the depths of all local events used in this study. The histogram bin width is 10 km.

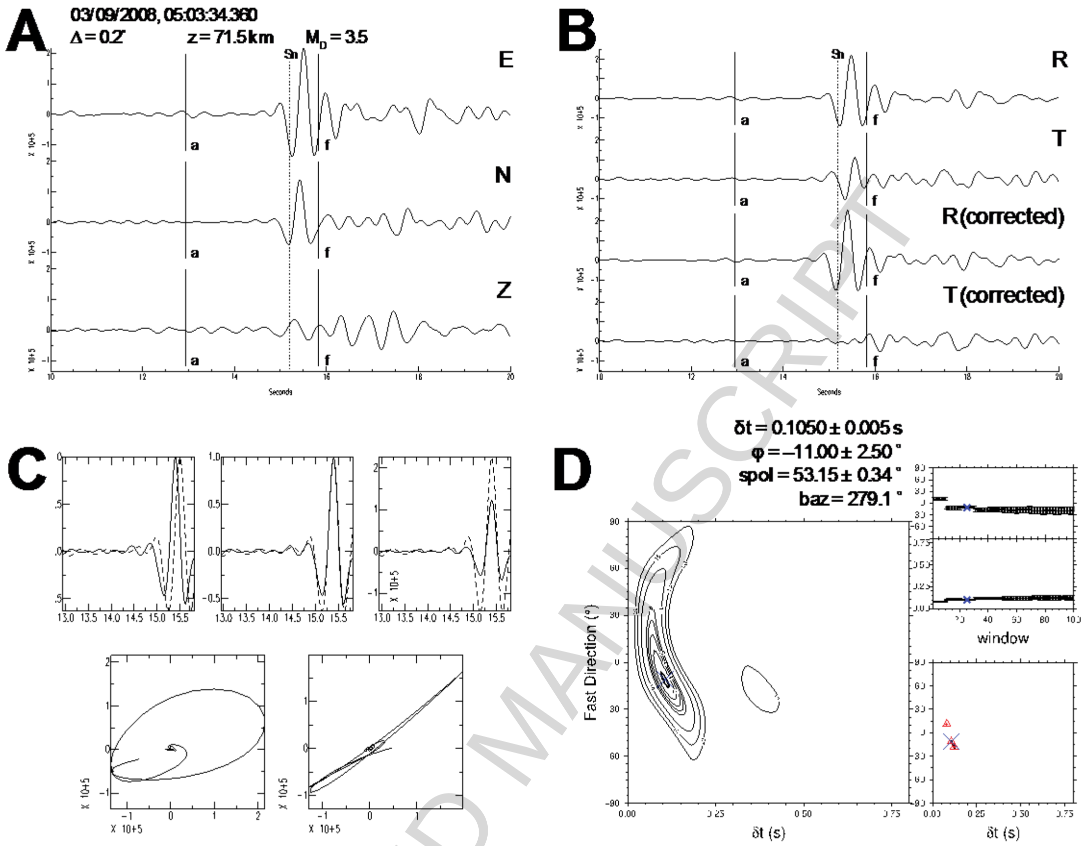

Figure 4: Example of a local S-splitting measurement at station ANWB (Barbuda) on a magnitude 3.5 event recorded on 03/09/2008, 05:03:34.360. The local event (17.70˚N, 67.64˚W, distance: 0.2˚) originated at a depth of 71.5 km. The data is filtered (0.5–2.5 Hz). See caption of Figure 2 for more details. For local splitting measurements the source polarisation in general is not aligned with the backazimuth. R and T do not represent radial and transverse components to the backazimuth but are rotated with respect to the initial source polarisation of the shear-wave.

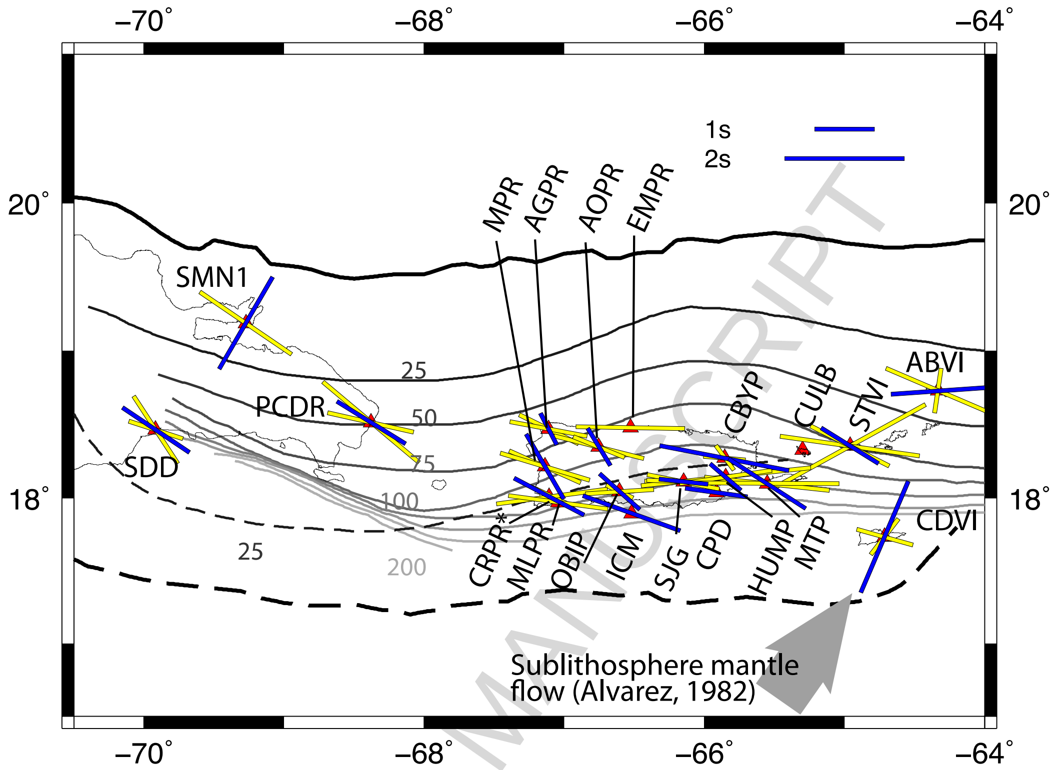

Figure 5: Stacked SK(K)S-splitting measurements in the NCPBZ from this work (blue bars) and previous studies (yellow bars). The length of the bar is proportional to the magnitude of the splitting (δt) and the orientation represents the angle (φ). Previous results were obtained by Russo et al. (1996), Piñero-Feliciangeli & Kendall (2008) and Benford et al. (2012), Meighan & Pulliam (2013) and Hodges & Miller (2015). Details can be found in Table 1. Note that the previous result shown at station CRPR is a result of station MGP located close-by and plotted on the locations of that station. The slab contours indicate the Puerto Rico Trench (solid) and the Los Muertos Trench (dashed) and are taken from Dolan et al. (1998). The thick lines show the 0 km contour lines, the thinner contours have an interval of 25 km. The grey arrow indicates sublithosphere mantle flow as proposed by Alvarez (1982). For individual SK(K)s-splitting measurements of these stations see Supplementary Figure 1.

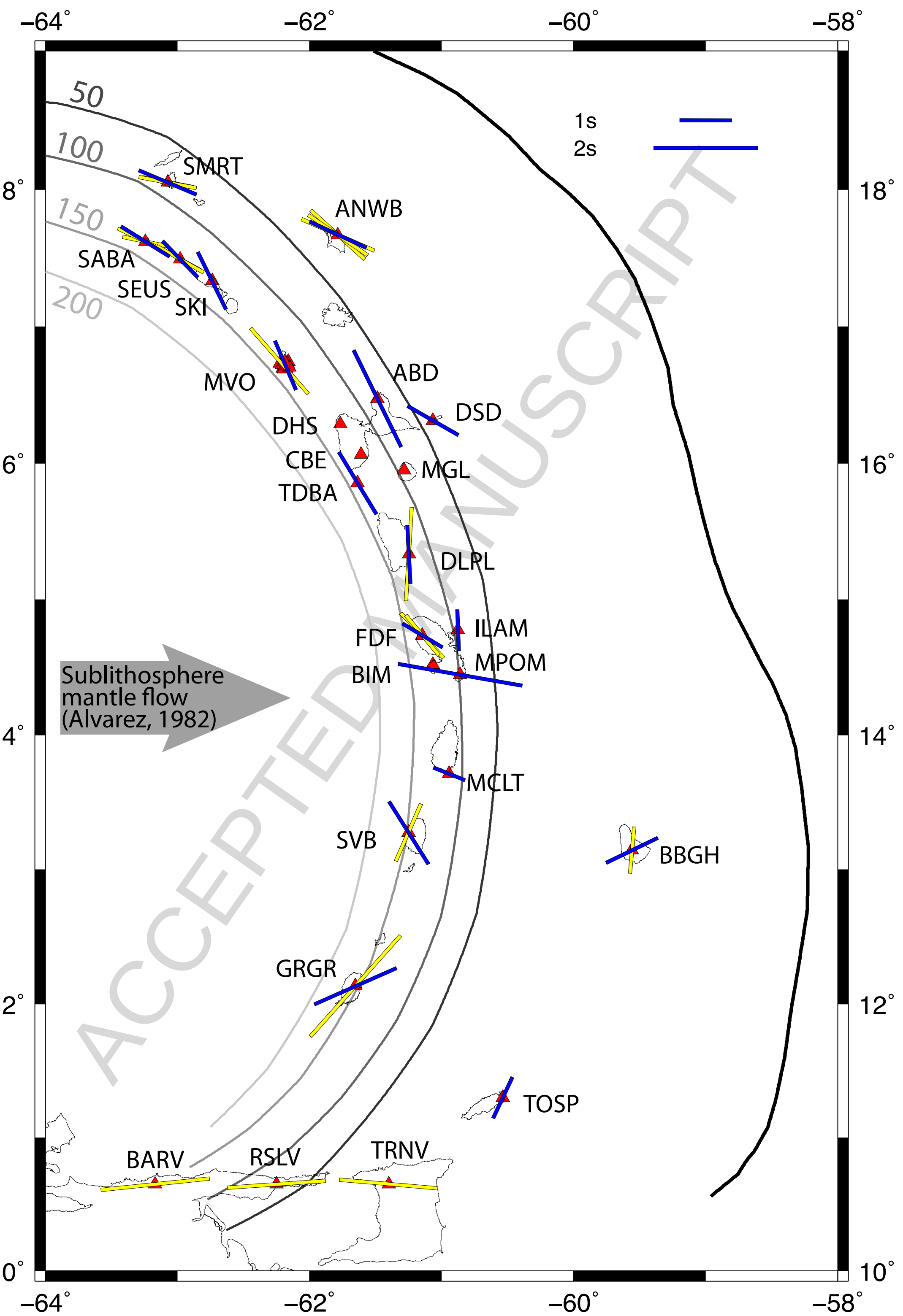

Figure 6: Stacked SK(K)S-splitting measurements in the LAA from this work (blue bars) and previous studies (yellow bars). The length of the bar is proportional to the magnitude of the splitting (δt) and the orientation represents the angle (φ). Previous results were obtained by Russo et al. (1996), Benford et al. (2012), Meighan & Pulliam (2013) and Hodges & Miller (2015). Details can be

found in Table 1. Note that MVO consists of a stack of individual stations. The slab contours are taken from Gudmundsson & Sambridge (1998). The thick line shows the 0 km contour line, the thinner contours have an interval of 50 km. The grey arrow indicates sublithosphere mantle flow as proposed by Alvarez (1982). For individual SK(K)s-splitting measurements of these stations see Supplementary Figure 2.

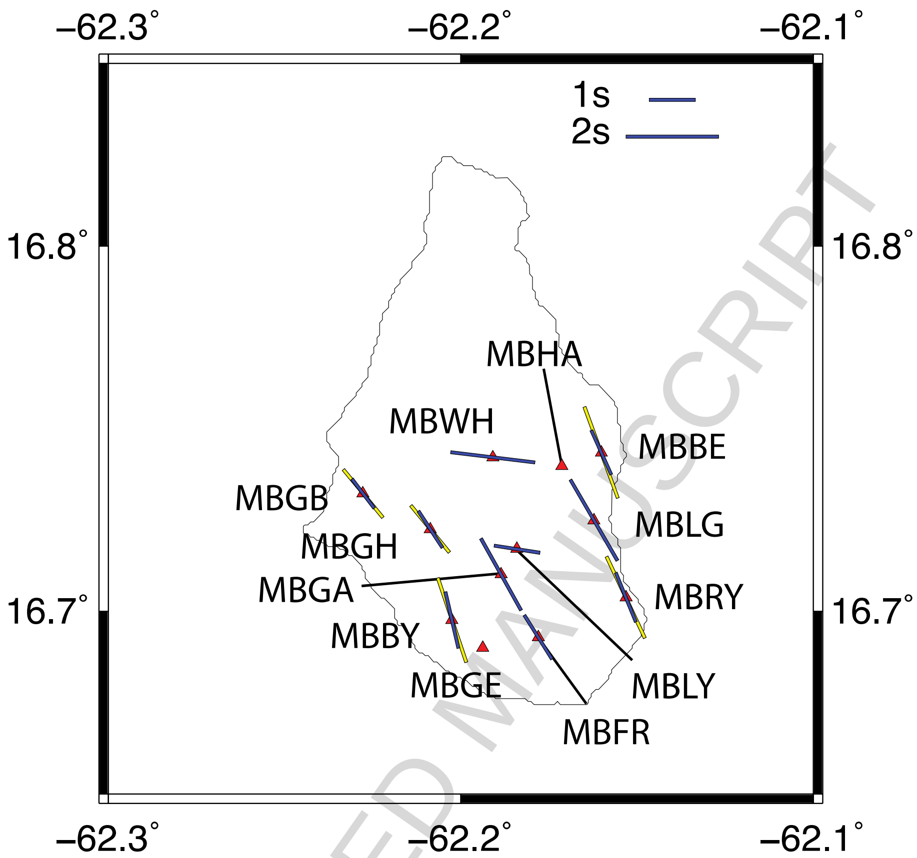

Figure 7: Stacked SKS-splitting measurements on individual stations on Montserrat from this work (blue bars) and previous studies (yellow bars). The length of the bar is proportional to the magnitude of the splitting (δt) and the orientation represents the angle (φ). All previous results were obtained by Piñero-Feliciangeli & Kendall (2008). For individual SK(K)s-splitting measurements of these stations see Supplementary Figure 3.

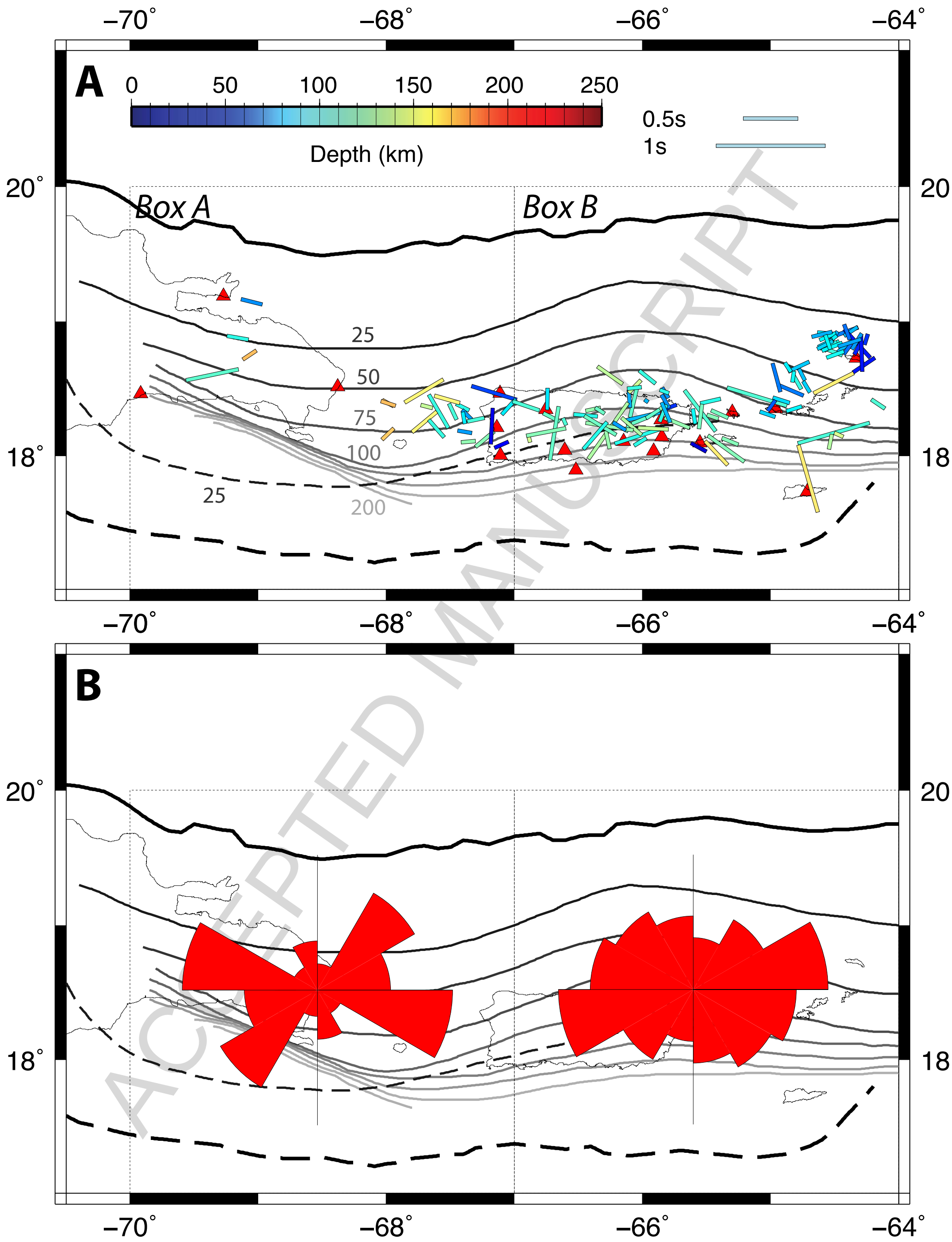

Figure 8: Local S-splitting measurements in the NCPBZ. A) Individual results of each measurement. The length of the bar is proportional to the magnitude of the splitting (δt) and the orientation represents the angle (φ). The colour of the bar indicates the event depth. The results are located on the midpoint of the ray path. Note that the ray path is assumed to be a straight line. This will introduce a location uncertainty. Due to the curvature of the ray path the midpoint of the path will be closer to the station. For local waves this effect can be neglected. The

boxes ("Box A" and "Box B"; dotted lines) are used as individual areas in Figure 10. The slab contours indicate the Puerto Rico Trench (solid) and the Los Muertos Trench (dashed) and are taken from Dolan et al. (1998). The thick lines show the 0 km contour lines, the thinner contours have an interval of 25 km. B) Rose diagrams showing the fast shear-wave polarisation for the local S-splitting measurements. Every rose diagram includes all local events located in the associated box (dotted lines). The lengths of the individual bars represent the normalised summation of all delay times in a particular orientation angle bin. The bin size is set to 30°.

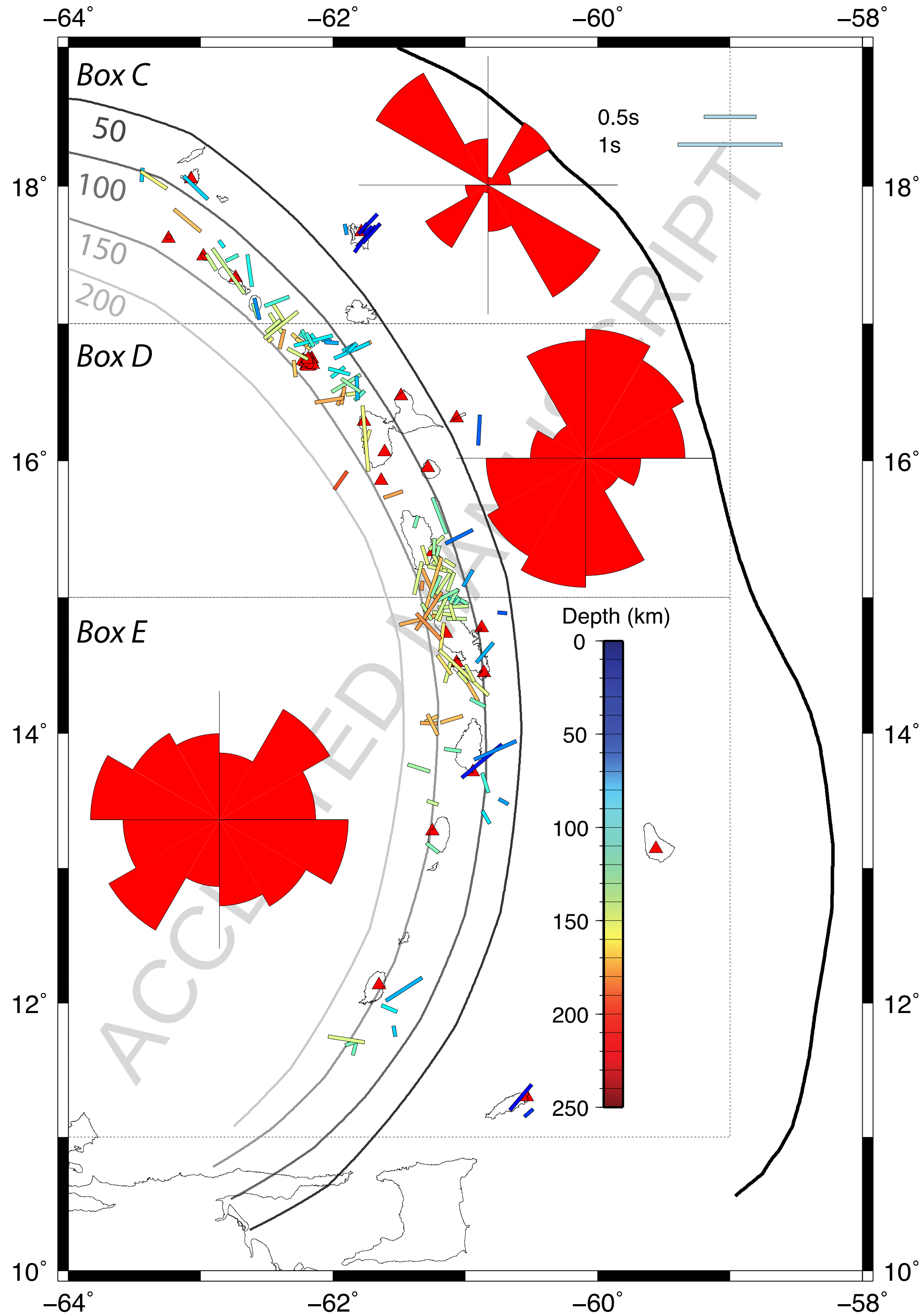

Figure 9: Local S-splitting measurements in the LAA. The length of the bar is proportional to the magnitude of the splitting (δt) and the orientation represents the angle (φ). The colour of the bar indicates the event depth. The results are located on the straight-line midpoint (see Figure 8 for explanation) of the ray path. The boxes ("Box C", "Box D" and "Box E"; dotted lines) are used as

individual areas in Figure 10. Every rose diagram includes all local events located in the associated box. The lengths of the individual bars represent the normalised summation of all delay times in a particular orientation angle bin. The bin size is set to 30°. The slab contours are taken from Gudmundsson & Sambridge (1998). The thick line shows the 0 km contour line, the thinner contours have an interval of 50 km.

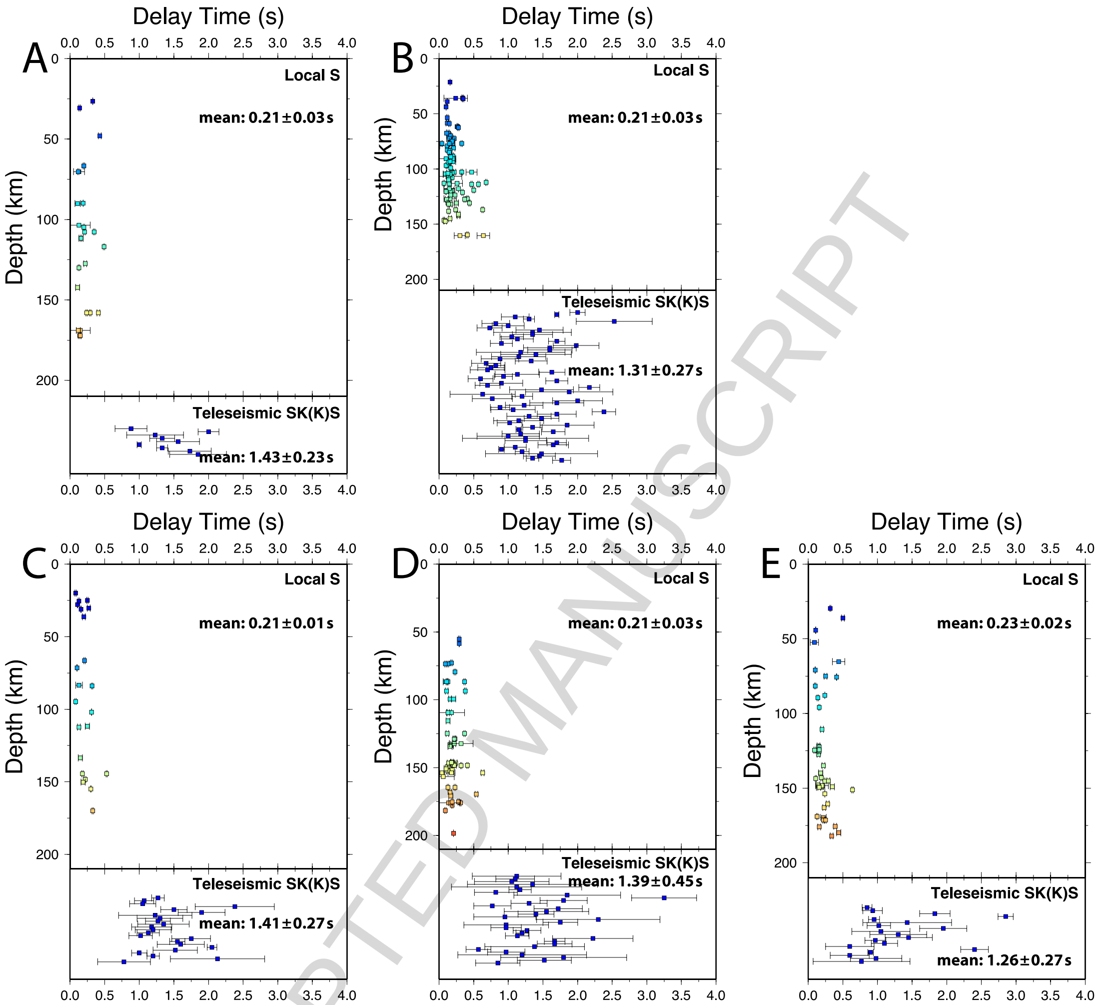

Figure 10: Shear-wave splitting delay times of different regions against event depth. The mean value and standard deviation are shown for S and SK(K)S in every plot. The local events are colour-coded according to their depths, matching the colours in Figures 8 and 9. Note that the depth information for the SKS-waves is arbitrary to facilitate visibility. Letters A to E represent the boxes in Figures 8A and 9: A) Greater Antilles – 17°N–20°N, 70°W–67°W. B) Greater Antilles – 17°N–20°N, 67°W–64°W. C) Lesser Antilles – 17°N–20°N, 64°W–59°W. D) Lesser Antilles – 15°N–17°N, 64°W–59°W. E) Lesser Antilles – 11°N–15°N, 64°W–59°W.

Highlights

We analyse the anisotropy around the Antilles subduction zone.

Shear-wave splitting indicates mostly trench-perpendicular orientation.

These are caused by anisotropy in or mantle flow beneath the subducting slab.

Two areas with anomalous trench-perpendicular orientation exist.

These are caused by eastward sublithospheric mantle flow through gaps in the slab.